

1 **Experimental study of non-Darcian flow characteristics in permeable stones**

2

3

4 A manuscript prepared for *Hydrology and Earth System Sciences*

5 by

6 Zhongxia Li<sup>1</sup>, Junwei Wan<sup>1</sup>, Tao Xiong<sup>1</sup>, Hongbin Zhan<sup>2\*</sup>, Linqing He<sup>3</sup>, Kun Huang<sup>1\*</sup>

7 <sup>1</sup>School of Environmental Studies, China University of Geosciences, 430074 Wuhan, China.

8 <sup>2</sup>Department of Geology and Geophysics, Texas A & M University, College Station, TX

9 77843-3115, USA.

10 <sup>3</sup>Changjiang Institute of Survey Technical Research MWR, Wuhan, China.

11 \* Corresponding authors:

12 Dr. Hongbin Zhan (zhan@~~geos~~.tamu.edu);

13 Dr. Kun Huang (cugdr\_huang@cug.edu.cn).

14

15

16

17

18

19

20

21 **Abstract**

22 This study provides experimental evidence of Forchheimer flow and transition between  
23 different flow regimes from the perspective of pore size of permeable stone. We have firstly  
24 carried out the seepage experiments of permeable stones with four different mesh sizes,  
25 including 24 mesh size, 46 mesh size, 60 mesh size, and 80 mesh size, which corresponding  
26 to mean particle sizes (50% by weight) of 0.71 mm, 0.36 mm, 0.25 mm, and 0.18 mm. The  
27 seepage experiments show that obvious deviation from Darcian flow regime is visible. In  
28 addition, the critical specific discharge corresponding to the transition of flow regimes (from  
29 pre-Darcian to post-Darcian) increases with the increase of particle sizes. When the “pseudo”  
30 hydraulic conductivity ( $K$ ) (which is computed by the ratio of specific discharge and the  
31 hydraulic gradient) increases with the increase of specific discharge ( $q$ ), the flow regime is  
32 denoted as the pre-Darcian flow. After the specific discharge increases to a certain value, the  
33 “pseudo” hydraulic conductivity begins to decrease, and this regime is called the post-  
34 Darcian flow. In addition, we use the mercury injection experiment to measure the pore size  
35 distribution of four permeable stones with different particle sizes, and the mercury injection  
36 curve is divided into three stages. The beginning and end segments of the mercury injection  
37 curve are very gentle with relatively small slopes, while the intermediate mercury injection  
38 curve is steep, indicating that the pore size in permeable stones is relatively uniform. The  
39 porosity decreases as the mean particle sizes increases, and the mean pore size can faithfully  
40 reflect the influence of particle diameter, sorting degree and arrangement mode of porous  
41 medium on seepage parameters. This study shows that the size of pores is an essential factor  
42 for determining the flow regimes. In addition, the Forchheimer coefficients are also discussed  
43 in which the coefficient  $A$  (which is related to the linear term of the Forchheimer equation) is  
44 linearly related to  $1/d^2$  as  $A = 0.0025(1/d^2) + 0.003$ ; while the coefficient  $B$  (which is related  
45 to the quadratic term of the Forchheimer equation) is a quadratic function of  $1/d$  as

46  $B = 1.14E-06(1/d)^2 - 1.26E-06(1/d)$ . The porosity ( $n$ ) can be used to reveal the effect of  
47 sorting degree and arrangement on seepage coefficient. The larger porosity leads to smaller  
48 coefficients  $A$  and  $B$  under the condition of the same particle size.

49 **Keywords:** permeable stone, mercury injection experiment, pore size, flow regime, non-  
50 Darcian flow.

## 51 1. Introduction

52 [Darcy \(1857\)](#) conducted a steady-state flow experiment in porous media and concluded  
53 that the specific discharge was proportional to the hydraulic gradient, which is the Darcy's  
54 law described as follow:

$$q = KJ \quad (1-1)$$

55 where  $q$  is the specific discharge,  $J$  is the hydraulic gradient, and  $K$  is the hydraulic  
56 conductivity. However, when the specific discharge increases above a certain threshold,  
57 deviation from Darcy's law is evident and the flow regime changes from Darcian flow regime  
58 to the so called non-Darcian flow regime ([Bear, 1972](#)), which was first observed by  
59 [Forchheimer \(1901\)](#), who proposed a widely used non-Darcian flow equation (the  
60 Forchheimer equation) as follow:

$$J = Aq + Bq^2 \quad (1-2)$$

61 where  $A$  and  $B$  are constants related to fluid properties and pore structure. The first and  
62 second terms on the right side of Eq. (1-2) roughly reflect the contributions of viscous and  
63 inertial forces (or resistance to flow), respectively.

64 From the Forchheimer equation, we can see that when the specific discharge is  
65 sufficiently small, the inertial force can be ignored, and the equation is transformed to the

66 form of Darcy's law. On the other hand, when the specific discharge is sufficiently large, the  
67 viscous force can be ignored, and the equation is transformed to the fully developed turbulent  
68 flow.

69 In addition to the polynomial function such as the Forchheimer equation, there are also  
70 several power-law functions proposed to describe the non-Darcian flow, and one of the most  
71 commonly used power-law equations is the Izbash equation ([Izbash, 1931](#)), which is written  
72 as:

$$J = aq^b \quad (1-3)$$

73 where  $a$  and  $b$  are the empirical parameters that depend on flow and materials properties, and  
74 the coefficient  $b$  is usually between 1 and 2.

75 Because of its applicability for a wide range of velocity spectrum and its sound physics,  
76 many scholars have adopted the Forchheimer equation (among many different types of  
77 equations) to explore the non-Darcian flow. Besides, the theoretical background of the  
78 Forchheimer equation has been discussed in details ([Panfilov and Fourar, 2006](#)). Numerous  
79 experimental data have confirmed the validity of the Forchheimer equation for a variety of  
80 nonlinear flow phenomena ([Geertsma, 1974](#); [Scheidegger, 1957](#); [Wright, 1968](#)). The  
81 quadratic Forchheimer law has also been revealed as a result of numerical modelling by  
82 simulating the Navier–Stokes flow in corrugated channels ([Koch and Ladd, 1996](#); [Skjetne et](#)  
83 [al., 1999](#); [Souto and Moyne, 1997](#)). To sum up, the Forchheimer equation will be selected as  
84 a representative to describe non-Darcy flow in this study.

85 Since the transition between Darcian flow and non-Darcian flow is important and  
86 difficult to quantify, different scholars have carried out experiments using a wide range of  
87 porous media, including homogeneous and heterogeneous porous media. Most of the  
88 experimental studies have focused on the influence of mean particle size on flow state

89 transition using homogeneous porous media. In fact, it was believed that the nonlinear (or  
90 non-Darcian) flow behavior in porous media was due to turbulent effect of flow in earlier  
91 studies and the Reynold number ( $Re$ ) was widely used to quantify the initiation of non-  
92 Darcian flow. [Bear \(1972\)](#) concluded that the critical  $Re$  (denoted as  $Re_c$ ) of flow states (or  
93 the  $Re$  value at which flow starts to change from Darcian flow regime to non-Darcian flow  
94 regime) is between 1 to 10. This finding was based on experimental data collected in packed  
95 sand beds ([Ergun, 1952](#); [Fancher and Lewis, 1933](#); [Lindquist, 1933](#); [Scheidegger, 1960](#)).  
96 [Schneebeli \(1955\)](#) and [Wright \(1968\)](#) experimentally measured the value of  $Re$  at the  
97 beginning of turbulence and concluded that at very high velocities, the deviation from  
98 Darcy's law is due to inertial effects followed by turbulent effects. In addition, [Dudgeon](#)  
99 [\(1966\)](#) confirmed that  $Re_c$  is about 60~150 for relatively coarse particle medium including  
100 river gravels, crushed rock particles and glass marbles with grain sizes from 16 mm to 152  
101 mm. [Dudgeon \(1966\)](#) indicated that the deviation from Darcy's law was not entirely due to  
102 turbulence, but in a large extent due to inertial forces. Besides, [Geertsma \(1974\)](#) proposed an  
103 empirical relationship among the inertial coefficient, permeability and porosity by conducting  
104 non-Darcian flow experiments in unconsolidated and consolidated sands. The laser  
105 anemometry and flow visualization studies of fluid flow in porous structures were used by  
106 [Dybbbs and Edwards \(1984\)](#), and they observed the nonlinear behavior at Reynolds numbers  
107 around 150. [Latifi et al. \(1989\)](#) found that the transition from unsteady-state laminar flow to  
108 non-Darcian flow in packed beds of spheres was between  $Re$  values of 110 and 370. [Seguin et](#)  
109 [al. \(1998\)](#) investigated the characterization of flow regimes in various porous media with  
110 electrochemical techniques and found that the end of the Darcian flow regime in packed beds  
111 of particles appeared at  $Re$  about 180. Besides, [Bu et al. \(2014\)](#) indicated that the Darcian  
112 flow in the packed beds would end at  $Re$  around 100 by using electrochemical techniques.  
113 [Sedghi-Asl et al. \(2014\)](#) found that the Darcy's law was usually not valid for rounded particle

114 sizes greater than 2.8 mm, according to the experimental results of flow in different sizes of  
115 rounded aggregates. Our previous experimental research ([Li et al., 2017](#)) indicated that when  
116 the particle size was smaller than 2.8 mm, the flow state gradually changed from pre-Darcy  
117 flow to post-Darcy flow when the specific discharge increased. When the medium particle  
118 sizes get even larger, such as 4.5 mm, 6.39 mm, 12.84 mm, and 16 mm ([Moutsopoulos et al.,  
119 2009](#)), only the post-Darcy flow exists. Based on above analysis, we can see that many  
120 previous experiments were carried out on homogeneous porous media, and the non-Darcy  
121 flow characteristics are quite different in porous media with various particle sizes.

122         Among the numerous experimental studies on this issue, it is evident that most of them  
123 focused on the effect of the mean particle size rather than the particle size distribution.  
124 Recently, a few investigators recognized the importance of particle size heterogeneity in  
125 understanding the transition of flow regimes, and have carried out a series of experiments to  
126 address the issue. For instance, [Van Lopik et al. \(2017\)](#) provided new experimental data on  
127 nonlinear flow behavior in various uniformly graded granular material for 20 samples,  
128 ranging from medium sands ( $d_{50} > 0.39$  mm) to gravel ( $d_{50} > 6.34$  mm). In addition, they  
129 investigated the nonlinear flow behavior through packed beds of 5 different types of natural  
130 sand and gravel from unconsolidated aquifers, as well as 13 different composite mixtures of  
131 uniformly graded filter sands at different grain size distributions and porosity values ([Van  
132 Lopik et al., 2019](#)). We have also discussed the effect of particle size distribution on  
133 Forchheimer flow and transition of flow regimes in a previous study ([Li et al., 2019b](#)). And  
134 our study showed that the uniformity coefficient of porous media (a term used to describe the  
135 pore size distribution) is a critical factor for determining the flow regimes besides the mean  
136 particle sizes. [Yang et al. \(2019\)](#) investigated the effects of the particle size distribution on the  
137 seepage behavior of a sand particle mixture subjected and evaluated the validity of empirical  
138 formulas of permeability and inertia factor used in engineering practice. [Shi et al. \(2020\)](#)

139 discussed the non-Darcy flow behavior of granular limestone with a wide range of porosity  
140 from 0.242 to 0.449. Based on the experimental data, [Shi et al. \(2020\)](#) proposed an empirical  
141 hydraulic conductivity-porosity relation as well as an expression of inertial coefficient.  
142 Regardless of the media investigated are homogeneous or heterogeneous, the essence of the  
143 water passing capacity of porous media is pore sizes. Thus, exploring the distribution of pores  
144 in porous media is the basis of studying flow dynamics of Darcian and non-Darcian flows.

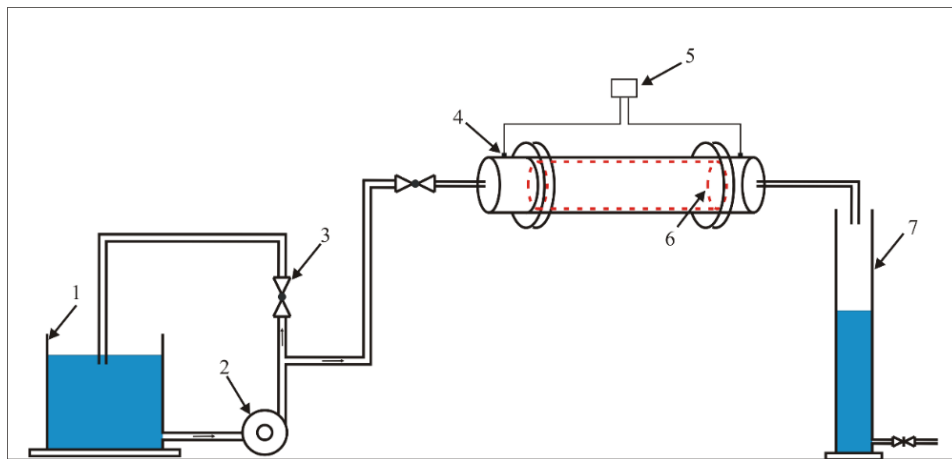
145 The purpose of this study is to provide a quantitative analysis on the effects of pore size  
146 on the transition of flow regimes between Darcian and non-Darcian flows based on a series of  
147 laboratory experiments. To meet the objectives, we have firstly carried out the seepage  
148 experiments of permeable stones with four different particle sizes. After that, we have  
149 conducted mercury injection experiments on permeable stones with four different particle  
150 sizes, and the pore size distributions with different particle sizes are obtained. Finally, the  
151 effect of pore size on the transition of flow regimes and Forchheimer coefficients are  
152 discussed based on the experimental results.

## 153 **2. Experimental methodology**

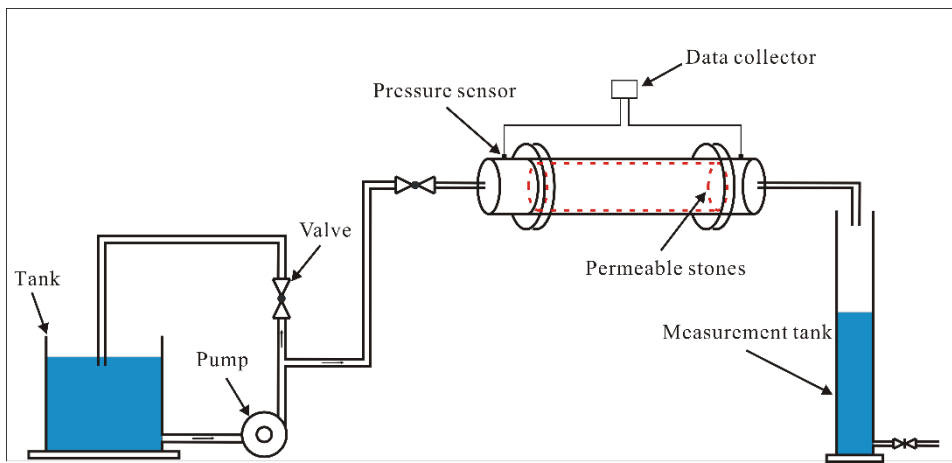
### 154 **2.1 Experimental setup and methods**

155 The experimental device is mainly composed of three parts: a water supply device, a  
156 seepage experimental device and a measuring device. The schematic diagram of the  
157 experimental apparatus is shown in Fig. 1. The water supply device consists of a tank, a  
158 centrifugal pump and a flow regulating valve. The seepage experimental device consists of a  
159 permeable stone and a plexiglass column. The measurement device monitors the real-time  
160 water temperature and pressure. The water temperature is measured using a thermometer with  
161 a precision of measurement of 0.1 °C. The water-level fluctuation is measured to calculate the  
162 flow rate by a pressure transducer (CY201, Chengdu test LLC, China) in the range of 0–20  
163 kPa with  $\pm 0.1\%$  accuracy. The measuring device consists of a cylindrical tank and a pressure

164 transducer. The sample of permeable stone is 60 mm in length with a circular cross section of  
 165 51.3 mm in diameter. Two pressure transducers are set at the entrance and exit of the column  
 166 to measure the pressure drop. To minimize the boundary effects, the pressure transducer is  
 167 placed 30 mm away from either end of the column, and the way of pressure measurement is  
 168 consistent with our previous studies ([Li et al., 2017](#); [Li et al., 2019b](#)).



169  
 170 ~~1) tank, 2) Pump, 3) Valve, 4) Pressure sensor, 5) Data collector, 6) Permeable stones, 7)~~  
 171 ~~Measurement tank.~~



172  
 173 Fig. 1 The schematic diagram of experimental apparatus.

174 **2.2 Experimental Materials and Procedures**

175 Four different particle sizes of permeable stones are selected to carry out the seepage  
 176 experiment in this study. It is necessary to make a brief overview of the preparation process



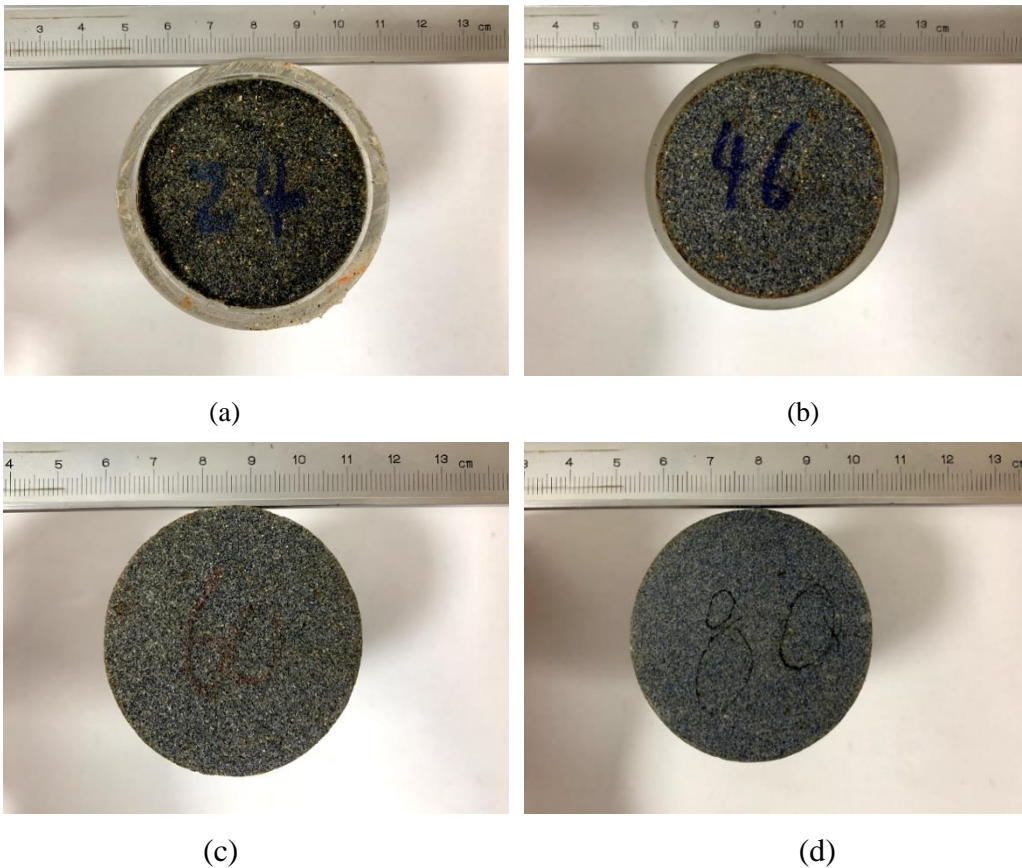
177 of permeable stone, which is a type of artificially made tight porous medium formed by sand  
178 grains and cementing compound. In the process of preparing permeable stone, a certain  
179 particle size of sand and cementing compound is put in a mold, and is consolidated at room  
180 temperature. Permeable stone is widely used in urban road design, sponge city construction  
181 and ecological effect research (Guan et al., 2021; Li et al., 2019a; Yu et al., 2021). And the  
182 most commonly used permeable base materials are large pore cement stabilized macadam,  
183 large diameter permeable asphalt mixture and so on (Suo et al., 2021). For permeable stone,  
184 there must be a certain connected pore space to maintain a certain permeability for  
185 transmitting water. However, the increase of pore space will lead to the decrease of pavement  
186 performance and mechanical strength (Han et al., 2016; Wang et al., 2021). Therefore, many  
187 scholars have carried out a lot of research on controlling the proper pore space of permeable  
188 stone (Alvarez et al., 2010; Prowell et al., 2002; Xie and Watson, 2004). We have carried out  
189 the seepage experiments of permeable stones with four different mesh sizes, including 24  
190 mesh size, 46 mesh size, 60 mesh size, and 80 mesh size, and the mesh size is defined as the  
191 number of mesh elements (all in square shapes) in a one inch by one inch square, thus a  
192 greater number of mesh size implies a smaller particle size. For instance, we can convert  
193 above four different mesh sizes of permeable stones into corresponding particle sizes of 0.71  
194 mm, 0.36 mm, 0.25 mm and 0.18 mm, respectively. The pore structure of permeable rock will  
195 not change in the process of the seepage experiment under room temperature, and the  
196 physical diagrams of four kinds of permeable stones with different particle sizes are shown in  
197 Fig. 2 and Fig. 3.



198

199

Fig. 2 Physical drawing of permeable stones with four different particle sizes.



200

201

202

203

204

205

Fig. 3 Permeable stones with different particle sizes: (a) 24 mesh size or 0.71 mm, (b) 46 mesh size or 0.36 mm, (c) 60 mesh size or 0.25 mm, and (d) 80 mesh size or 0.18 mm.

206

207

208

209

It is worth mentioning that the contact surface of the sample and the plexiglass column is sealed to prevent any preferential flow through the wall of the plexiglass column. After the permeable stone is inserted into the plexiglass column, both ends are sealed with silicone glue. The water passing through the permeable stone is then collected by a cylindrical tank.

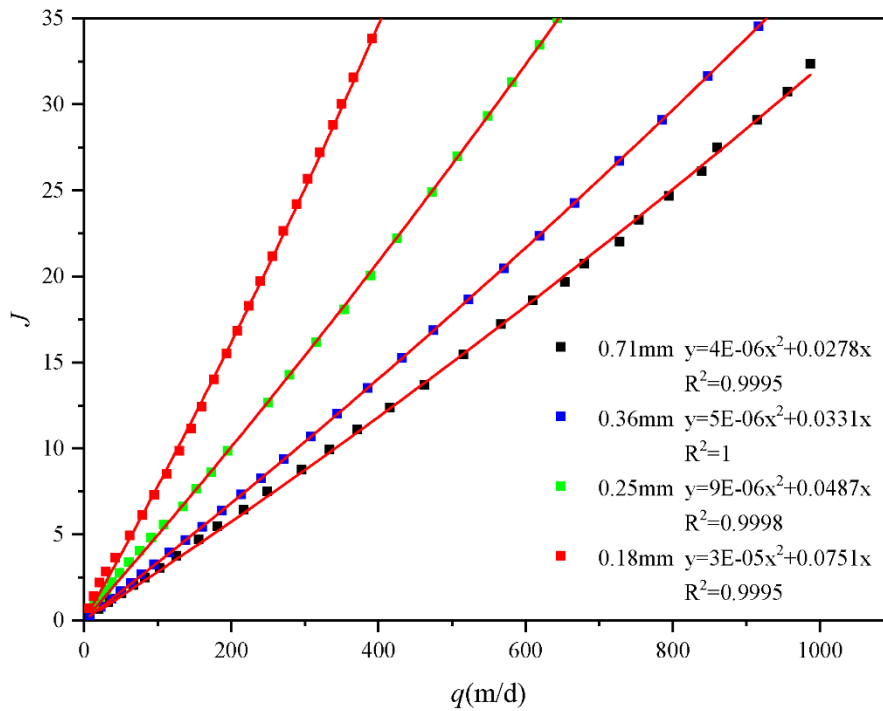
210 Moreover, the ratio of the internal diameter of the column to the particle size of permeable  
211 stone is greater than 12, which can eliminate any possible wall effect on the seepage  
212 according to [Beavers et al. \(1972\)](#). When carrying out the experiment, it usually takes about  
213 two hours to saturate the permeable stone. For each packed sample, more than 25 tests with  
214 different constant inlet pressures were conducted under steady-state flow condition. In  
215 addition, for each group of permeable stone, repeated tests under the same experimental  
216 condition were carried out 3-4 times to ensure the accuracy of the results.

### 217 **3. Results and discussion**

#### 218 **3.1 Permeable stone seepage experiment**

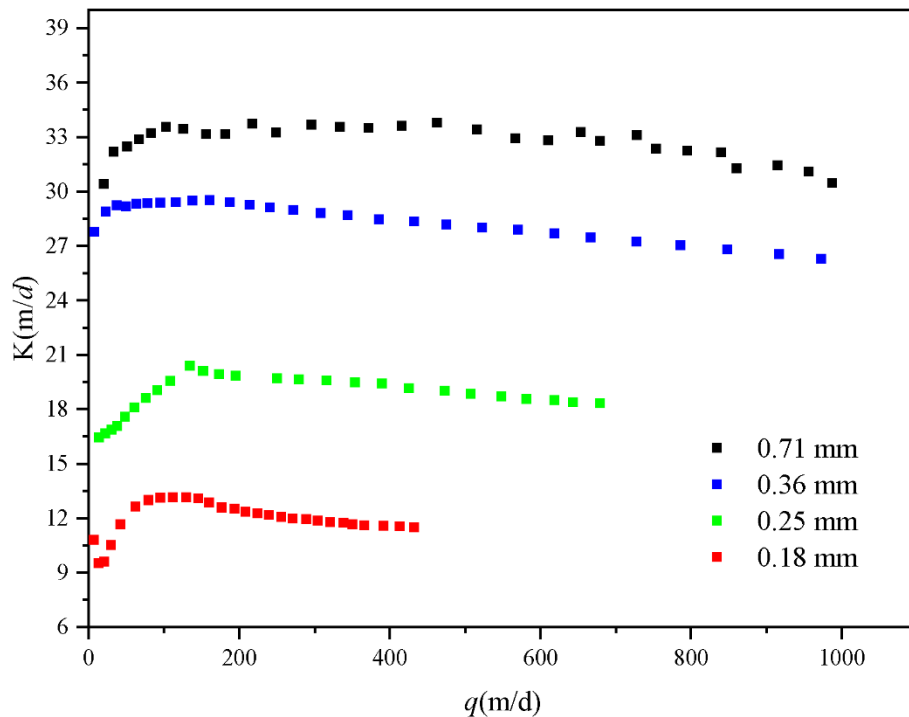
219 In this study, we selected permeable stone with four different particle sizes as the  
220 research objects, including 24 mesh size, 46 mesh size, 60 mesh size and 80 mesh size. The  
221 mesh size is the number of holes per inch of screen mesh and the particle size is inversely  
222 proportional to the mesh size. The mean particle sizes corresponding to the four different  
223 mesh sizes are 0.71 mm, 0.36 mm, 0.25 mm, and 0.18 mm, respectively, where the mean  
224 particle size is corresponding to 50% by weight hereinafter in this study. Such a definition of  
225 mean particle size may be different from some other studies such as [Fetter \(2001\)](#) which has  
226 used 10% by weight as the mean particle size. The relationship between the specific  
227 discharge ( $q$ ) and the hydraulic gradient ( $J$ ) of permeable stones is plotted in Fig. 4. The units  
228 of specific discharge mentioned in this study are all converted to meters per day (m/d). To  
229 better compare with the actual groundwater flow, we converted the specific discharge to  
230 meters per day (m/d). Therefore, the best-fitting exercise yields Forchheimer numbers with  
231 orders of magnitudes to be about -4. In addition, the critical Forchheimer numbers proposed  
232 by Zeng and Grigg (2006) and Javadi et al. (2014) are empirical, in fact, the transition  
233 between Darcy to non-Darcy is successional over a certain range of Forchheimer numbers.  
234 The non-Darcian flow criterion applicable to different pore media is established by

235 conducting seepage resistance experiments in homogeneous and heterogeneous porous media  
 236 in our previous study (Li et al., 2017; Li et al., 2019b), which is consistent with the results of  
 237 Zeng and Grigg (2006). Generally speaking, the  $q$ - $J$  and  $q$ - $K$  curves are the most commonly  
 238 used methods to analyze flow regime when conducting seepage resistance experiments in  
 239 porous media. However, the nonlinear characteristics of  $q$ - $J$  curve are not obvious due to the  
 240 relatively small velocity range used in the experiments. The traditional hydraulic conductivity  
 241 is the ratio of the specific discharge versus the hydraulic gradient ( $q/J$ ), and it is a constant if  
 242 Darcy's law is applicable, which is denoted as  $K_D$  (Li et al., 2019b). In fact, the ratio of  $q/J$  is  
 243 no longer a constant for the problems discussed in this study. In a word, the  $q$ - $K$  curve can be  
 244 used to observe the transition of flow state more intuitively.



245  
 246 Fig. 4 Variation of  $J$  with  $q$  of four permeable stones with different particle sizes.  
 247 Fig. 4 shows that when  $q$  is somewhat the same, a larger mesh size (which means a  
 248 smaller particle size) will lead to a larger  $J$ . And the results are consistent with our previous  
 249 studies (Huang et al., 2013; Li et al., 2017; Li et al., 2019b). However, the nonlinear  
 250 characteristics of  $q$ - $J$  curve are not obvious due to the relatively small velocity range used in

251 the experiments. Nevertheless, the best-fitting results using the Forchheimer equation are  
 252 satisfactory. To analyze the influence of pore size on seepage flow regimes, we have obtained  
 253 the relationship between  $q$  and the “pseudo” hydraulic conductivity ( $K$ ) (which is computed  
 254 using  $q/J$ ) of four permeable stones with different particle sizes, as shown in Fig. 5. We  
 255 should point out that the “pseudo” hydraulic conductivity term discussed here for non-  
 256 Darcian flow is usually not a constant, thus it is different from the hydraulic conductivity  
 257 term used in Darcy’s law, which is a constant. It is obvious that the hydraulic conductivity is  
 258 not a constant with the increase of specific discharge, so it is called the "pseudo" hydraulic  
 259 conductivity ([Li et al., 2019b](#)).



260

261 Fig. 5 Variation of  $K$  with  $q$  of four permeable stones with different particle sizes.

262 We can divide the  $q$ - $K$  curve into two segments: for the first segment,  $K$  increases with  
 263 the increase of  $q$ , which is denoted as the pre-Darcian flow. For the second segment, after  $q$   
 264 increases to a certain value,  $K$  begins to decrease with  $q$ , which is called the post-Darcian

265 flow. In fact, Izbash (1931) presented the equation as  $q = M \left( \frac{dH}{dx} \right)^m = Mi^m$ , where  $M$  and  $m$

266 are the coefficients determined by fluid flow and properties of porous media. When  $m=1$ , the  
 267 Izbash equation reduces to Darcy law, when  $m>1$ , the Izbash equation corresponds to the pre-  
 268 Darcy flow and when  $m<1$ , the Izbash equation refers to the post-Darcy flow (Dejam et al.,  
 269 2017; Soni et al., 1978). Besides, Dejam et al. (2017) carried out a more detailed study on  
 270 issues related to the pre-Darcy and post-Darcy flows. And the influence of pre-Darcy flow on  
 271 the pressure diffusion for homogenous porous media is studied in terms of the nonlinear  
 272 exponent and the threshold pressure gradient. When the hydraulic gradient is small (and  $q$  is  
 273 small as well), a great portion of water is bounded (or becomes immobile) on the surface of  
 274 solids due to the solid-liquid interfacial force, and only a small fraction of the water is mobile  
 275 and free to flow through the pores. In addition, another justification for the pre-Darcy  
 276 behavior may be due to an effect of a stream potential which generates small countercurrents  
 277 along pore walls in a direction opposite that of the main flow (Bear, 1972; Scheidegger, 2020).  
 278 And Swartzendruber (1962b) stated that the surface forces arose in a solid-fluid interface due  
 279 to strong negative charges on clay particle surfaces and the dipolar nature of water molecules  
 280 caused a pressure gradient response to be nonlinear and led to the pre-Darcy flow  
 281 (Swartzendruber, 1962a). As the hydraulic gradient increases (and  $q$  increases as well), the  
 282 initial threshold for mobilizing the previously immobile water near the solid-liquid surface is  
 283 overcome and more water participates in the flow. For this reason, the "pseudo" hydraulic  
 284 conductivity increases with the increase of hydraulic gradient and the specific discharge in  
 285 the first segment. When the specific discharge increases to the critical specific discharge ( $q_c$ ),  
 286 the "pseudo" hydraulic conductivity is maximized. According to  $K = \frac{q}{Aq + Bq^2} = \frac{1}{A + Bq}$   
 287 based on Eq. (1-2), we can find that the "pseudo" hydraulic conductivity begins to decrease  
 288 as the specific discharge continues to increase. Besides, the critical specific discharge  
 289 corresponding to the transition of flow regimes (from pre-Darcian to post-Darcian) increases

290 with the increase of particle sizes (or decrease of mesh sizes).

### 291 **3.2 Mercury injection experiment**

292 The particle size, different grain size distributions and degree of sorting are the main  
293 factors that determine the size and shape of pores. And the shape of the pores determines the  
294 tortuosity and distribution of flow paths, which are related to viscous and inertial flow  
295 resistances. It is generally accepted in previous studies that the pore sizes of porous media  
296 have an impact on the seepage law ([Maalal et al., 2021](#); [Zhou et al., 2019](#)). However, the  
297 structure of natural porous media is very complex, and it is difficult to quantify the effects of  
298 the arrangement of particles on the seepage law. The characteristics of pore size distribution  
299 contains critical information for quantifying the flow regimes. The mercury intrusion  
300 porosimetry and the nitrogen adsorption isotherm are two commonly used methods to  
301 characterize the pore sizes and their distribution ([Rijfkogel et al., 2019](#)). Besides, other  
302 techniques can also be used to derive the pore size distribution, such as small-angle neutron  
303 and X-ray scattering measurements, CT images and nuclear magnetic resonance ([Anovitz and](#)  
304 [Cole, 2015](#); [Hall et al., 1986](#); [Kate and Gokhale, 2006](#); [Lindquist et al., 2000](#)). In this study  
305 we will use the mercury injection experiment to measure the pore size distribution of the four  
306 permeable stones with different particle sizes and use the information to describe the flow  
307 regimes.

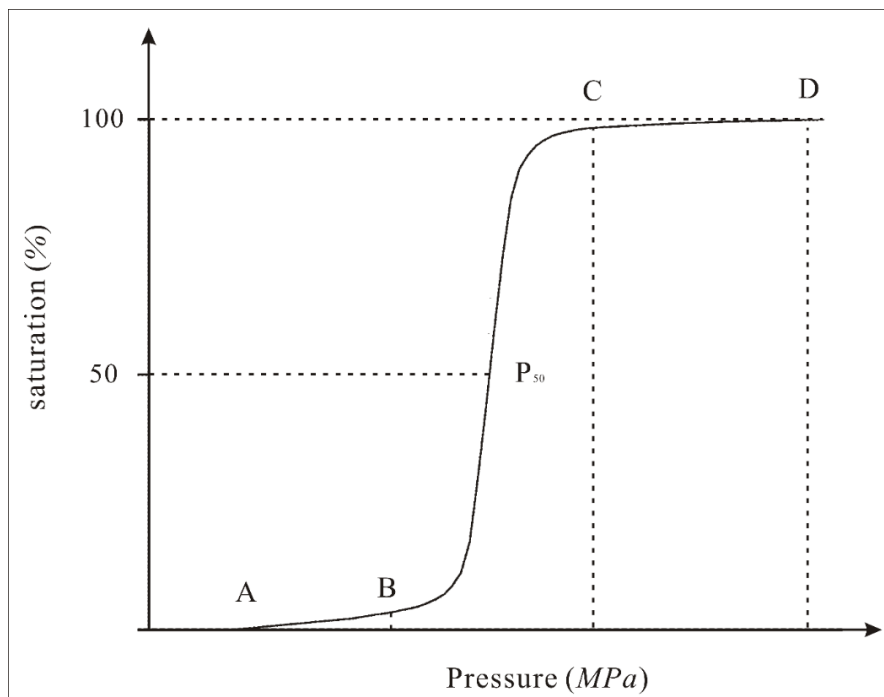
308 To quantitatively study the pore size and pore throat distribution, we need to envisage a  
309 physically based conceptual model to describe the pore structures of permeable stones. The  
310 commonly used model is the so-called capillary model ([Pittman, 1992](#); [Rezaee et al., 2012](#);  
311 [Schmitt et al., 2013](#)), which approximates the connected pores as many paralleled capillaries.  
312 And the capillary forces are generated at the phase interface due to the surface tension  
313 between the solid and liquid phases when liquid flows in a capillary. The capillary force is  
314 directed toward the concave liquid level, and is shown as ([Washburn, 1921](#)):



$$P_c = \frac{2\sigma \cos \theta}{r} \quad (3-1)$$

315 where  $P_c$  is the capillary force,  $\sigma$  is the solid-liquid interfacial tension,  $\theta$  is the wet angle  
 316 between the liquid and the solid surface, and  $r$  is the radius of curvature in capillary.

317 Since mercury is a nonwetting phase to solids, so to get mercury into the pores of the  
 318 permeable stone, an external force (or displacement pressure) must be applied to overcome  
 319 the capillary force. When a greater pressure is applied, mercury can enter smaller pores.  
 320 When a certain pressure is applied, the injection pressure is equivalent to the capillary  
 321 pressure in the corresponding pore. Then we can calculate the corresponding capillary radius  
 322 according to Eq. (3-1), and the volume of mercury injected is the pore volume.



323

324 Fig. 6 Schematic diagram of pressure changes with saturation: the initial stage (A-B), the  
 325 intermediate mercury entry stage (B-C), and the end stage (C-D).

326 By continuously increasing the injection pressure, one can obtain the curve of injection  
 327 pressure and the volume of injected mercury, from which one can also obtain the pore-throat  
 328 distribution curve and capillary pressure curve. According to the amount of mercury injected

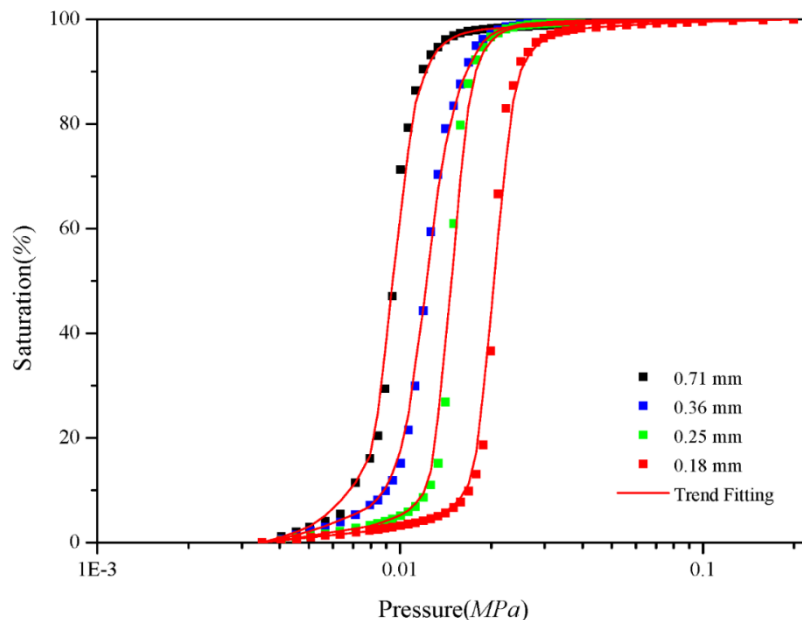


329 at different injection pressures, the relation between the injection pressure and the injection  
330 saturation is shown in Fig. 6.

331 Fig. 6 shows that the mercury injection curve can be divided into three stages. Firstly,  
332 during the initial stage (A-B) which has a very mild slope, the intake pressure is very small  
333 and the intake saturation is also very low. With the increasing of the injection pressure, the  
334 intake saturation slowly increases. Secondly, during the intermediate mercury entry stage (B-  
335 C) which has a steep slope, a small pressure change will lead to a significant saturation  
336 change. This means that the pores are relatively uniform and the differences in pore sizes are  
337 small. It is well known that for mercury injection experiments, as injection pressure increases,  
338 the injection saturation will gradually increase and eventually all the pores will be filled with  
339 mercury. As can be seen from Fig. 7, with the continuous injection of mercury, the pressure of  
340 permeable stones with different particle sizes varies with saturation, which is reflected in the  
341 different pressure  $P_B$  and  $P_C$  at different stages. However, the reason for the different pressure  
342 is the difference of pore size distribution in the permeable stones. Therefore, the pressure  
343 ratio of B and C ( $P_C/P_B$ ) can be used as one of the criteria to characterize the heterogeneity of  
344 pore size in porous media. Besides, when the saturation reaches 50%, the corresponding  
345 pressure value ( $P_{50}$ ) reflects the characteristics of the mean pore size, and a larger  $P_{50}$  leads to  
346 a larger mean pore size. Finally, during the end stage (C-D) which has a very mild slope as  
347 well, the amount of mercury will not increase considerably when the injection pressure  
348 increases. This indicates that nearly all the pores are essentially filled with mercury, and the  
349 mercury injection experiment is completed. After completing the mercury injection  
350 experiments, we have obtained the mercury injection curves of four permeable stones with  
351 different particle sizes, as shown in Fig. 7.

352 We can make a number of interesting observations based on Fig. 7. Firstly, the pressure  
353 at the starting point (when the saturation begins to increase), denoted as  $P_A$ , increases as the

354 mean particle size decreases. This means that the maximum pore size in permeable stone  
 355 decreases with the decrease of the mean particle sizes. Secondly, the mercury injection curves  
 356 of four permeable stones all include steep intermediate stages, indicating that the pore size  
 357 distributions are all relatively uniform. And the corresponding pressure values at points B and  
 358 C increase as the mean particle sizes decreases. Moreover, the pressure ratios corresponding  
 359 to points B and C ( $P_C/P_B$ ) also decrease with the decrease of particle sizes, suggesting even  
 360 more uniform pore size distributions with decreasing particle sizes. Thirdly, the intermediate  
 361 mercury entry stages gradually shift to the right with the decrease of particle sizes. When the  
 362 saturation reaches 50%, the corresponding pressure (the median pressure) decreases with the  
 363 increase of the mean particle sizes. Fourthly, the mercury injection curves of these four  
 364 permeable stones with different particle sizes all approach 100% saturation with very mild  
 365 slopes, indicating that there are few small pores in the permeable stones. We have extracted  
 366 the key pressure characteristic values of mercury injection experiment of Fig. 7, and listed the  
 367 results in Table 1.



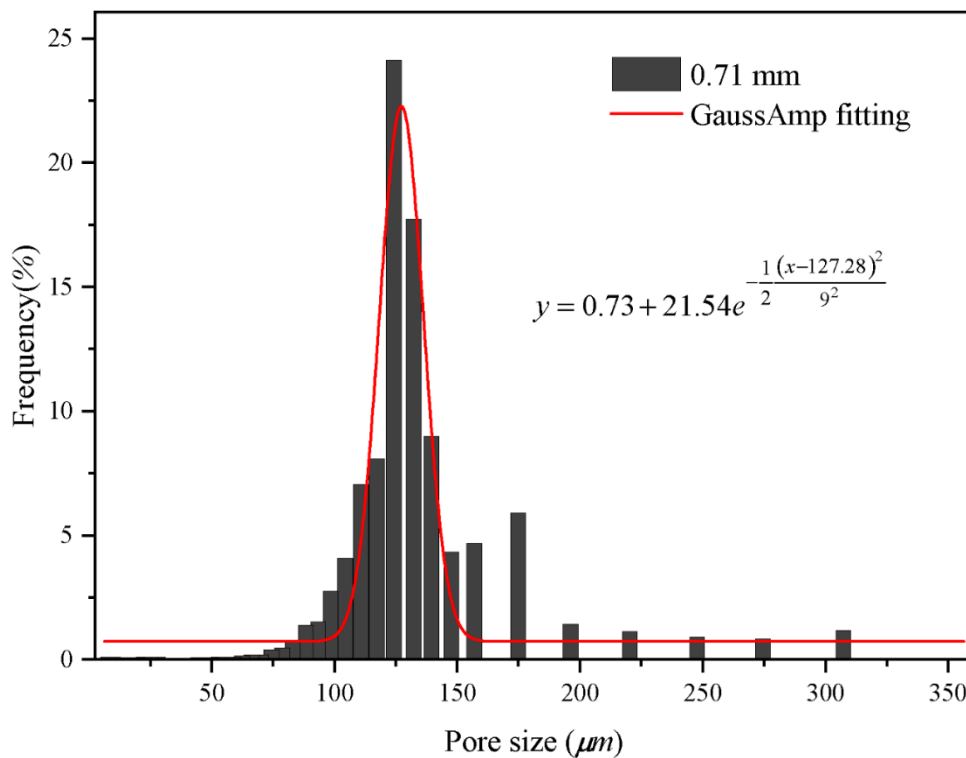
368

369 Fig. 7 Variation of pressure with saturation of four permeable stones with different particle  
 370 sizes.

371 Table 1. Pressure characteristic values of four permeable stones with different particle sizes.

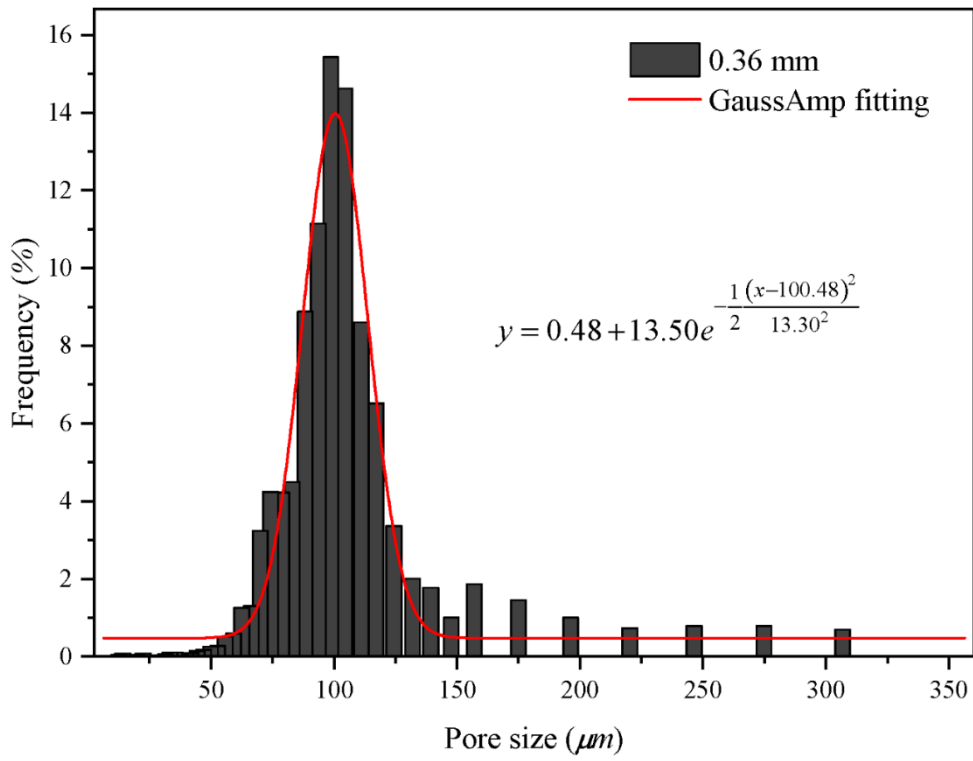
Mesh size	$P_A(MPa)$	$P_B(MPa)$	$P_C(MPa)$	$P_{50}(MPa)$	$P_C/P_B$
24	0.0041	0.0064	0.0133	0.0094	2.0987
46	0.0045	0.0071	0.0188	0.0119	2.6374
60	0.0051	0.0112	0.0211	0.0150	1.8764
80	0.0057	0.0158	0.0281	0.0211	1.7758

372 To observe the pore size distributions of the four permeable stones with different particle  
 373 sizes in more details, we can calculate the percentages of different pore sizes in permeable  
 374 stones according to the mercury injection curves, as shown in Figs. 8-11.



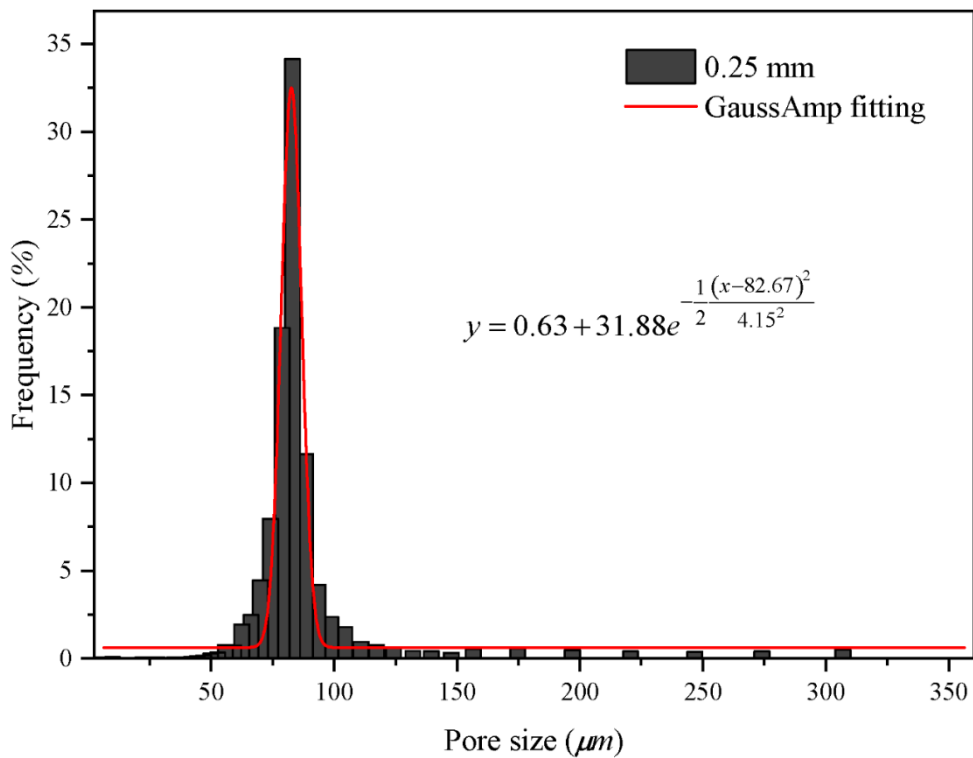
375  
 376 Fig. 8 Histogram of pore size distribution of permeable stone with diameter of 0.71 mm.

377



378

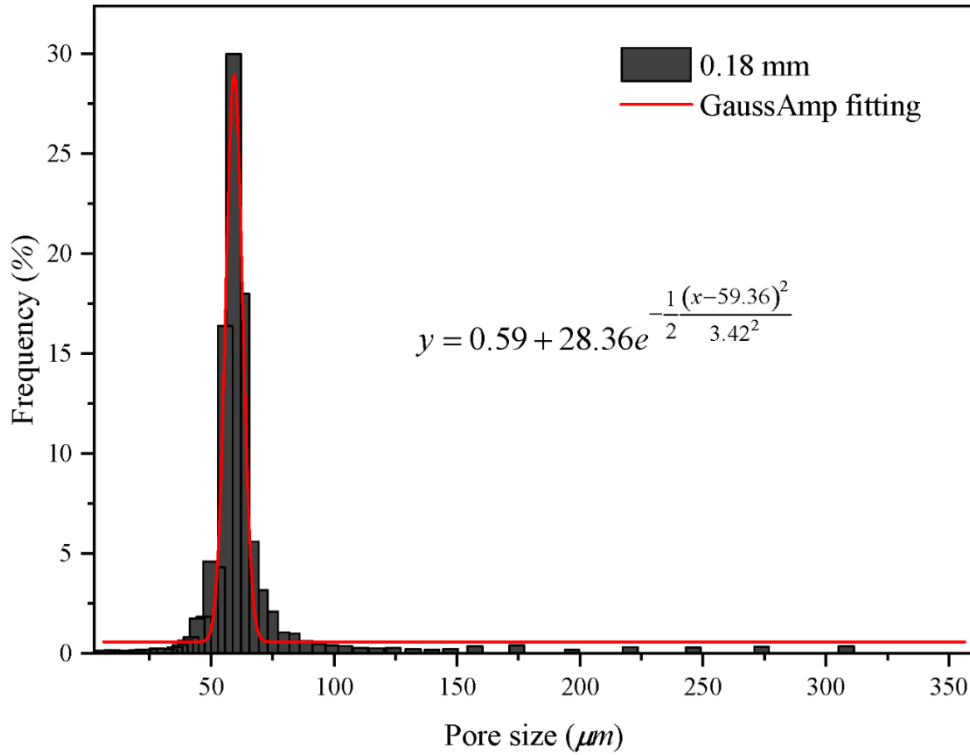
379 Fig. 9 Histogram of pore size distribution of permeable stone with diameter of 0.36 mm.



380

381 Fig. 10 Histogram of pore size distribution of permeable stone with diameter of 0.25 mm.

382



383

384 Fig. 11 Histogram of pore size distribution of permeable stone with diameter of 0.18 mm.

385 From Fig. 8 to Fig. 11 we can find that the pore sizes of the four permeable stones are  
 386 uniform and fall within narrow ranges. The pore size distributions of four different particle  
 387 sizes show a skewed normal distribution. Besides, the pore maximum proportion (the peak of  
 388 the curve, see Figs. 8-11) of permeable stones with different particle sizes are different, which  
 389 are  $124 \mu\text{m}$ ,  $99 \mu\text{m}$ ,  $83 \mu\text{m}$  and  $59 \mu\text{m}$ , respectively. The Gaussian function is widely used to  
 390 characterize the pore system and classify the petrophysical rock ([Harlan et al., 1995](#); [Jeon et](#)  
 391 [al., 2014](#); [Xu and Torres-Verdín, 2013](#)), and the general form of the Gauss function is shown  
 392 below:

$$y = y_0 + He^{-\frac{(x-x_c)^2}{2w^2}} \quad (3-2)$$

393 where  $H$  is the height of the peak of the mercury injection curve,  $x_c$  is the abscissa  
 394 corresponding to the peak of the curve (the pore size),  $w$  is the standard variance, which  
 395 represents the width of the curve. To characterize the distribution of pore structure of four

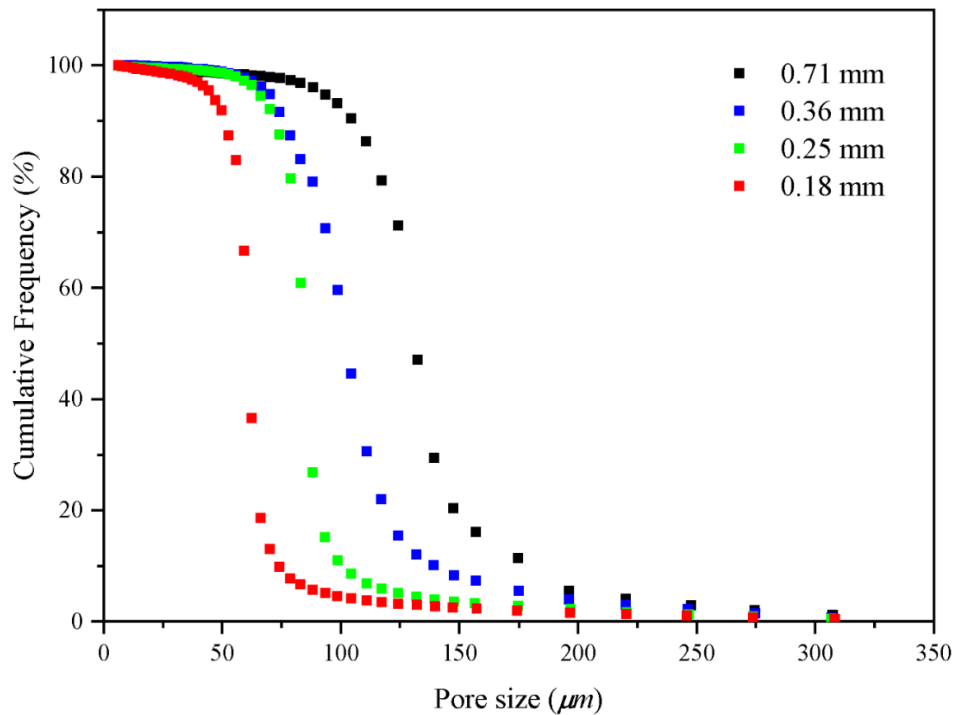
396 different permeable stones, we best-fit the Gaussian curve of the pore distribution of four  
 397 permeable stones with different particle sizes, and the best-fitted parameters are shown in  
 398 Table 2. We can make several interesting observations from Table 2. Firstly, the expected  
 399 value ( $x_c$ ) decreases with decreasing particle sizes of permeable stone, and the  $x_c$  values of  
 400 different permeable stones are almost the same. Secondly, the standard variance ( $w$ )  
 401 corresponding to the permeable stone of 0.18 mm is the smallest, indicating that the pore size  
 402 distribution is more concentrated (or relatively homogeneous). For comparison, the pore size  
 403 distribution of 0.36 mm permeable stone is the widest with the greatest variance. Finally,  
 404 different values of  $H$  represent different proportions of pore sizes, among which the highest  
 405 proportion can reach 34.04%. It will be desirable to establish a correlation between the  
 406 parameters used in the pore-size distribution of Eq. (3-2) with the two Forchheimer  
 407 coefficients  $A$  and  $B$ . This objective may be achieved using high-resolution pore-scale fluid  
 408 mechanics simulations, which are out of the scope of this study. Further research is needed to  
 409 address this issue in the future.

410 Table 2. Gaussian function characteristic values of four permeable stones with different  
 411 particle sizes.

Mesh size	particle size (mm)	$y_0$	$H$	$x_c$	$w$
24	0.71	0.73	21.54	127.28	9.00
46	0.36	0.48	13.49	100.48	13.30
60	0.25	0.63	31.88	82.67	4.15
80	0.18	0.59	28.36	59.36	3.42

412 The pore size distributions fall within ever narrower ranges with mesh sizes become  
 413 larger. Moreover, the cumulative percentage frequency curves of the pore size distributions

414 with different particle sizes are exhibited in Fig. 12 and the results are shown in Table 3.



415

416 Fig. 12. The cumulative frequency curve of pore size distribution.

417 Fig. 12 shows that  $R_{50}$  (the pore size corresponding to the median pressure  $P_{50}$ ) increases  
418 with the increase of permeable stone particle size, and the mean pore diameter ( $R_m$ ) also  
419 increases. In general, the pore size corresponding to the median pressure (denoted as  $R_{50}$ )  
420 may be slightly different than the mean pore diameter ( $R_m$ ) which has been defined in  
421 different ways by various investigators when analyzing the pore size distributions ([Hea and](#)  
422 [Zhangb, 2015](#); [Zhen-Hua et al., 2007](#); [Zhihong et al., 2000](#)). As  $R_{50}$  is easily identifiable in  
423 the mercury injection experiments, it is used in this study as a representative of the mean pore  
424 diameter ( $R_m$ ) of the permeable stone. Besides, the seepage law of permeable stone is closely  
425 related to the pore size, and the smaller average pore size will result in a larger hydraulic  
426 gradient under the condition of the same specific discharge (see Fig. 4). The pore size  
427 characteristic values with different particle sizes are listed in Table 3. We find that the  
428 porosity decreases as the particle size increases while the mean pore diameter increases. And  
429 the mean pore size can reflect the influence of particle diameter, sorting degree and

430 arrangement mode of porous medium on seepage parameters.

431 Table 3. Pore size characteristic values of four permeable stones with different particle sizes.

Mesh size	Mean particle size (mm)	Porosity (%)	$R_m$ ( $\mu m$ )	$R_{50}$ ( $\mu m$ )
24	0.71	32.35	131.31	131.34
46	0.36	36.69	102.56	103.42
60	0.25	40.82	84.73	85.09
80	0.18	42.88	60.97	61.12

432 *Note:*  $R_m$  is the mean pore diameter,  $R_{50}$  is the pore diameter corresponding to the median  
433 pressure  $P_{50}$ .

### 434 3.3 Analysis of influencing factors of Forchheimer equation coefficients

#### 435 3.3.1 Influence of particle size on equation coefficient

436 The analysis of non-Darcy coefficient has always been of interest to many researchers  
437 working in different disciplines of porous media flow ([Moutsopoulos et al., 2009](#); [Sedghi-Asl  
438 et al., 2014](#); [Shi et al., 2020](#)). Various studies have suggested expressions for Forchheimer  
439 coefficients, different scholars obtained numerous datasets through different experiments and  
440 simulation methods to quadratic best-fitting the specific discharge-hydraulic gradient curves.  
441 And the coefficients of different fitting equations are shown in the following Table 4. Ward  
442 (1964) proposed the estimation formula of Forchheimer coefficients  $A$  and  $B$  by analyzing the  
443 experimental data of 20 different porous media:

$$A = \frac{360}{gd^2} \quad B = \frac{10.44}{gd} \quad (3-3)$$



444 where  $d$  is the particle diameter hereinafter,  $g$  is the acceleration due to gravity. Based on  
 445 the mixed model of parallel capillary tubes, Blick (1966) proposed a new form of  
 446 Forchheimer coefficients:

$$A = \frac{32}{gn d^2} \quad B = \frac{C_D}{2gn^2 d} \quad (3-4)$$

447 where  $n$  is the porosity of the medium,  $C_D$  is an appropriate phenomenological  
 448 coefficient.

449 Besides, Ergun (1952) suggested the new expressions by extending the classic Kozeny-  
 450 Carman model:

$$A = \frac{150(1-n)^2}{gn^3 d^2} \quad B = \frac{1.75(1-n)}{gn^3 d} \quad (3-5)$$

451 Kovács (1981) analyzed 300 data in the range of  $10 < Re < 100$ , and derived a similar  
 452 expression for the case of dispersed spherical particles, and the coefficients of Forchheimer  
 453 are as follows:

$$A = \frac{144(1-n)^2}{gn^3 d^2} \quad B = \frac{2.4(1-n)}{gn^3 d} \quad (3-6)$$

454 Kadlec and Knight (1996) also proposed the following Forchheimer coefficients:

$$A = \frac{255(1-n)^2}{gn^{3.7} d^2} \quad B = \frac{2(1-n)}{gn^3 d} \quad (3-7)$$

455  
 456 **Table 4.** The Forchheimer coefficients of empirical relations.

<u>Equations</u>	<u>Coefficient A (s/m)</u>	<u>Coefficient B (s<sup>2</sup>/m<sup>2</sup>)</u>
------------------	----------------------------	--

<a href="#">Ward (1964)</a>	$A = \frac{360}{gd^2}$	$B = \frac{10.44}{gd}$
<a href="#">Blick (1966)</a>	$A = \frac{32}{gnd^2}$	$B = \frac{C_D}{2gn^2d}$
<a href="#">Ergun (1952)</a>	$A = \frac{150(1-n)^2}{gn^3d^2}$	$B = \frac{1.75(1-n)}{gn^3d}$
<a href="#">Macdonald et al. (1979)</a>	$A = \frac{180(1-n)^2}{gn^{3.6}d^2}$	$B = \frac{1.8(1-n)}{gn^{3.6}d}$
<a href="#">Kovács (1981)</a>	$A = \frac{144(1-n)^2}{gn^3d^2}$	$B = \frac{2.4(1-n)}{gn^3d}$
<a href="#">Kadlec and Knight (1996)</a>	$A = \frac{255(1-n)^2}{gn^{3.7}d^2}$	$B = \frac{2(1-n)}{gn^3d}$
<a href="#">Irmay (1964)</a>	$A = \frac{180(1-n)^2}{gn^3d^2}$	$B = \frac{0.6(1-n)}{gn^3d}$

457 [Sidiropoulou et al. \(2007\)](#) focused on the determination of the Forchheimer coefficients  
458 for non-Darcian flow in porous media and evaluated the original theoretical equations above  
459 and the validity of these equations was checked using existing experimental data. In addition,  
460 the Root Mean Square Error (RMSE) was used as a criterion to quantitatively evaluate the

461 coefficients, and the RMSE was defined as  $RMES = \sqrt{\frac{\sum_{i=1}^N (x_i - y_i)^2}{N}}$ , where  $x_i$  were the  
462 experimental values of Forchheimer coefficients,  $y_i$  were the values computed by different  
463 equations above, and  $N$  was the total number of experimental points ([Moutsopoulos et al.,](#)  
464 [2009](#)). The different forms of Forchheimer coefficients described above are based on different  
465 assumptions and simplifications of pore structure. Consequently, these series of coefficients  
466 are applicable under specific conditions with different degrees of accuracy.

467 According to Eq. (1-2), the hydraulic gradient ( $J$ ) is composed of a viscous force-related  
468 component ( $J_n$ ) and an inertia force-related component ( $J_r$ ), ~~as below~~ and for specific  
469 derivation, please refer to previous studies ([Huang, 2012](#)):

$$J_n = Aq = \frac{\alpha\mu}{\rho g} \frac{1}{d^2} q \quad J_r = \frac{\beta}{g} \frac{1}{d} q^2 \quad (3-38)$$

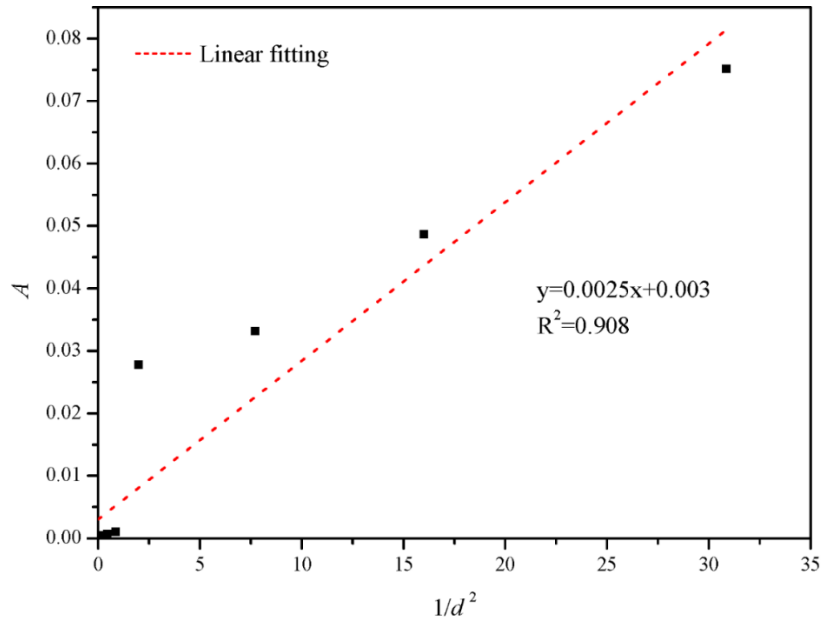
470 We can see from Eq. (3-38) that the  $J_n$  is inversely proportional to the square of the particle  
 471 size, and the  $J_r$  is inversely proportional to the particle size when the specific discharge  
 472 remains the same. Both  $J_n$  and  $J_r$  are closely related to specific surface area and sizes of pores.  
 473 Therefore, the particle size is an important factor affecting the Forchheimer coefficient,  
 474 [Huang et al. \(2013\)](#) carried out the experimental investigation on water flow in four columns  
 475 with cubic arrays of acrylic balls in diameter 3 mm, 5 mm, 8 mm and 10 mm, where all the  
 476 acrylic balls are arranged in regular cubes. Accordingly, the coefficients  $A$  and  $B$  can be  
 477 written as follows:

$$A = \frac{\alpha\mu}{\rho g} \frac{1}{d^2} \quad B = \frac{\beta}{g} \frac{1}{d} \quad (3-49)$$

478 where  $\alpha$  and  $\beta$  are constants related to the shape, sorting, and arrangement of the particles,  
 479 and the specific derivation process is detailed in the previous study ([Huang, 2012](#)). The  
 480 experimental results showed that the coefficient  $A$  was inversely proportional to the particle  
 481 diameter square ( $d^2$ ) and coefficient  $B$  was inversely proportional to the particle size ( $d$ )  
 482 ([Huang et al., 2013](#)).

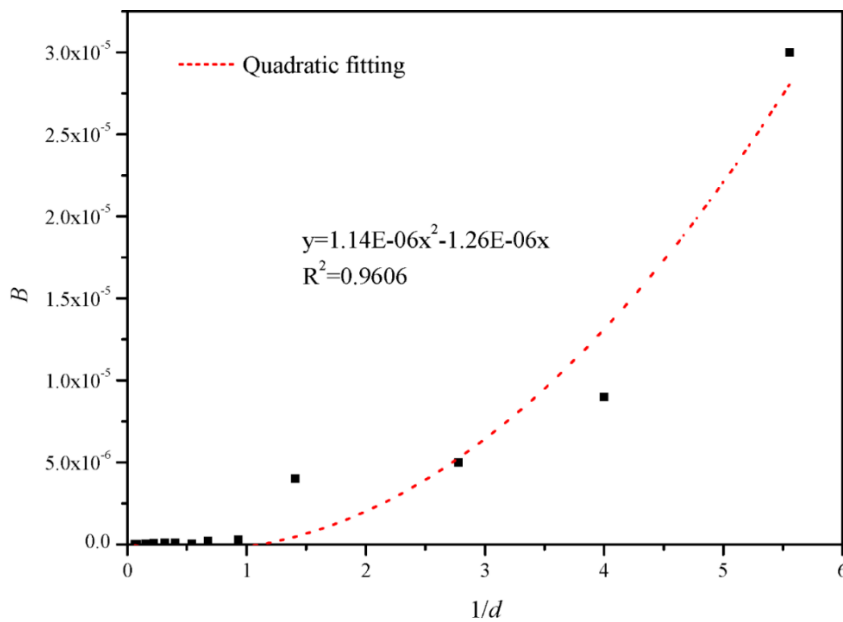
483 The uniform diameter cubic arrangement of porous media mentioned above is a rather  
 484 ideal medium. The shape and arrangement of particles of natural pore aquifers are usually  
 485 irregular. Therefore, the above-mentioned linear correlations between  $A$  and  $1/d^2$ , and  
 486 between  $B$  and  $1/d$  should be examined specifically. For this purpose, we collect the  
 487 experimental data of homogeneous porous media, including the previous research results and  
 488 the results of other scholars. Among them, samples P1-P4 are the permeable stones selected  
 489 in this study, samples L1-L5 are from previous studies ([Li et al., 2017](#)), and the experimental  
 490 data of samples M1-M4 are from [Moutsopoulos et al. \(2009\)](#). The fitting coefficients are

491 shown in Table 45. Furthermore, we can identify nice correlations between the Forchheimer  
 492 coefficient  $A$  and  $1/d^2$  and between the Forchheimer coefficient  $B$  and  $1/d$ , which are shown  
 493 in Fig. 13 and Fig. 14, respectively.



494

495 Fig. 13. Variation of  $A$  with  $1/d^2$  of different homogeneous particle sizes.



496

497 Fig. 14. Variation of  $B$  with  $1/d$  of different homogeneous particle sizes.

498 We can see from Fig. 13 that the coefficient  $A$  is linearly related to  $1/d^2$  and the

499 relationship between coefficient  $A$  and is given as  $A = 0.0025(1/d^2) + 0.003$ . And the  
500 relationship between coefficient  $B$  and  $1/d$  is completely different from the linear correlation  
501 as reported before. Fig. 14 shows that the coefficient  $B$  is quadratic related to  $1/d$  and the  
502 relationship between coefficient  $B$  and  $1/d$  is given as  $B = 1.14E-06(1/d)^2 - 1.26E-06(1/d)$ .  
503 That is to say, the relationship between coefficient  $A$  and  $1/d^2$  is consistent with the law of  
504 simple cubic arrangement porous media, but the relationship between coefficient  $B$  and  $1/d$  is  
505 not consistent with the law of simple cubic arrangement porous media. The structure of  
506 porous medium arranged in cubes is different from the permeable stone. The porosity of the  
507 porous media with spheres arranged in cubic is close to 0.48, independent of the diameter of  
508 spheres. While the particle shape, arrangement and tightness of permeable stone are different,  
509 and the porosity of permeable stone with different particle size is also different (see Table 3).

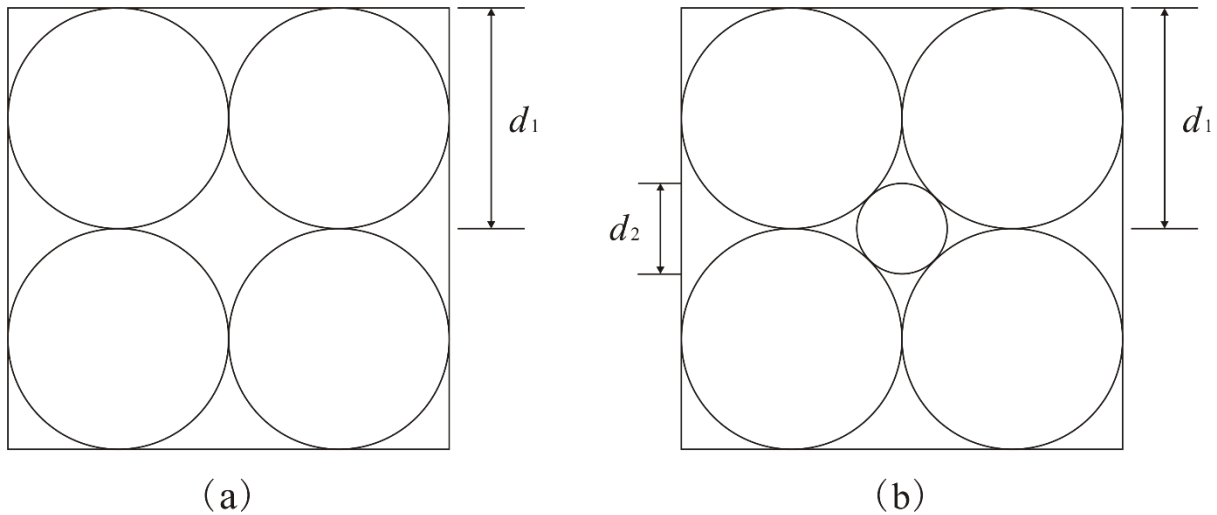
510 Table 45. Experimental fitting coefficient of different homogeneous particle sizes.

Sample	Particle size (mm)	Fitting equation	$A$	$B$	The correlation
P1	0.18	$y=0.0751x+3E-05x^2$	0.0751	3E-05	0.9995
P2	0.25	$y=0.0487x+9E-06x^2$	0.0487	9E-06	0.9998
P3	0.36	$y=0.0331x+5E-06x^2$	0.0331	5E-06	1
P4	0.71	$y=0.0278x+4E-06x^2$	0.0278	4E-06	0.9995
L1	1.075	$y=0.001x+3E-07x^2$	0.001	3E-07	0.9999
L2	1.475	$y=0.0007x+2E-07x^2$	0.0007	2E-07	0.9998
L3	1.85	$y=0.0005x+5E-08x^2$	0.0005	5E-08	0.9998
L4	2.5	$y=0.0005x+9E-08x^2$	0.0005	9E-08	0.9997

L5	3.17	$y=0.0004x+1E-07x^2$	0.0004	1E-07	0.9998
M1	4.5	$y=3E-05x+7E-08x^2$	3E-05	7E-08	0.9913
M2	6.39	$y=3E-05x+3E-08x^2$	3E-05	3E-08	0.9984
M3	12.84	$y=1E-05x+2E-08x^2$	1E-05	2E-08	0.9977
M4	16	$y=1E-05x+2E-08x^2$	1E-05	2E-08	0.998

### 511 3.3.2 Influence of porosity on equation coefficient

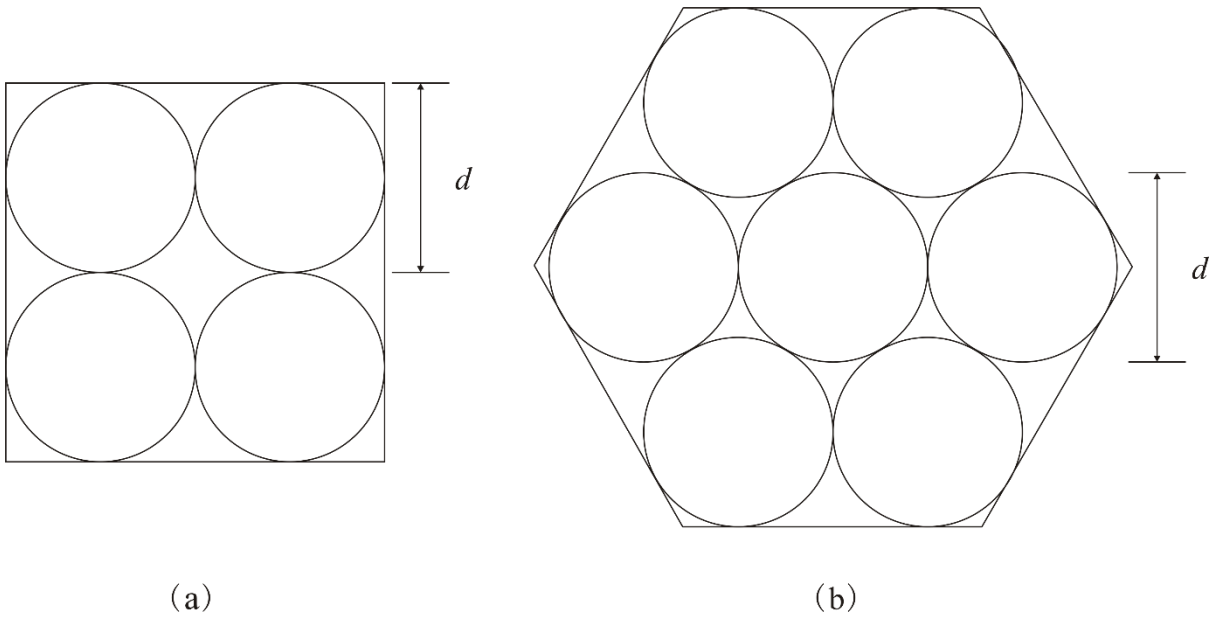
512 In above sections, we have analyzed the influence of particle sizes on seepage  
513 coefficient. Furthermore, the pore size and pore specific surface area are also related to the  
514 arrangement and sorting degree of particles, that is, to the porosity of porous media. To  
515 explore the effect of sorting degree on seepage coefficient, we draw a schematic diagram of  
516 different sorting degree of particles, as shown in Fig. 15. The degree of particle sorting is one  
517 of the important factors affecting the pore size. In porous media with a poor sorting degree,  
518 the pore size is usually determined by the diameter of the smallest particle. We can see from  
519 Fig. 15 that the pores between the larger particles are filled by smaller particles, resulting in  
520 even smaller pores. In addition, the poorer sorting degree of particles leads to the larger pore  
521 specific surface area and stronger viscous force of flow, which can lead to a larger coefficient  
522 A.



523 (a) 524 Fig. 15. The schematic diagram of particle sorting degree in different types.

525 Fig. 15. The schematic diagram of different particle sorting with cube arrangement.

526 Furthermore, we have also provided the schematic diagrams of spherical particles with  
 527 equal size in two simple arrangements, namely cube arrangement and hexahedron  
 528 arrangement, as shown in Fig. 16. And the cube arrangement is the less compact arrangement  
 529 with a pore diameter of  $0.414d$ , while the hexahedron arrangement is the more compact  
 530 arrangement with a pore diameter of  $0.155d$ . The characteristic value of pore structure in  
 531 different arrangement with the same particle size are shown in Table 56. We can see that  
 532 different arrangement modes will substantially affect the pore specific surface area and pore  
 533 size of porous media. The more compactly packed particles lead to the larger pore specific  
 534 surface area and stronger viscous force. Meanwhile, the smaller pore diameter is associated  
 535 with stronger effect of viscous force and inertia force. In summary, the better sorting degree  
 536 of particles leads to the weaker viscous and inertial forces, then the coefficients  $A$  and  $B$  will  
 537 be smaller. As the better sorting degree and the less compact (or looser) arrangement particles  
 538 mean the larger porosity, so we can conclude that the larger porosity leads to the smaller  
 539 coefficients  $A$  and  $B$  under the condition of the same particle size.



540

541

542

543

544

545

**Fig. 16. The schematic diagram of particle arrangement in different types.**

**Fig. 16. The schematic diagram of cube and hexahedron arrangement with the same particle size.**

Table 56. Characteristic value of pore structure in different arrangement with the same particle size.

Arrangement mode	Side length	Porosity (%)	Specific surface area
Cube	$2d$	47.60	3.142
Hexahedron	$1.577d$	43.30	3.402

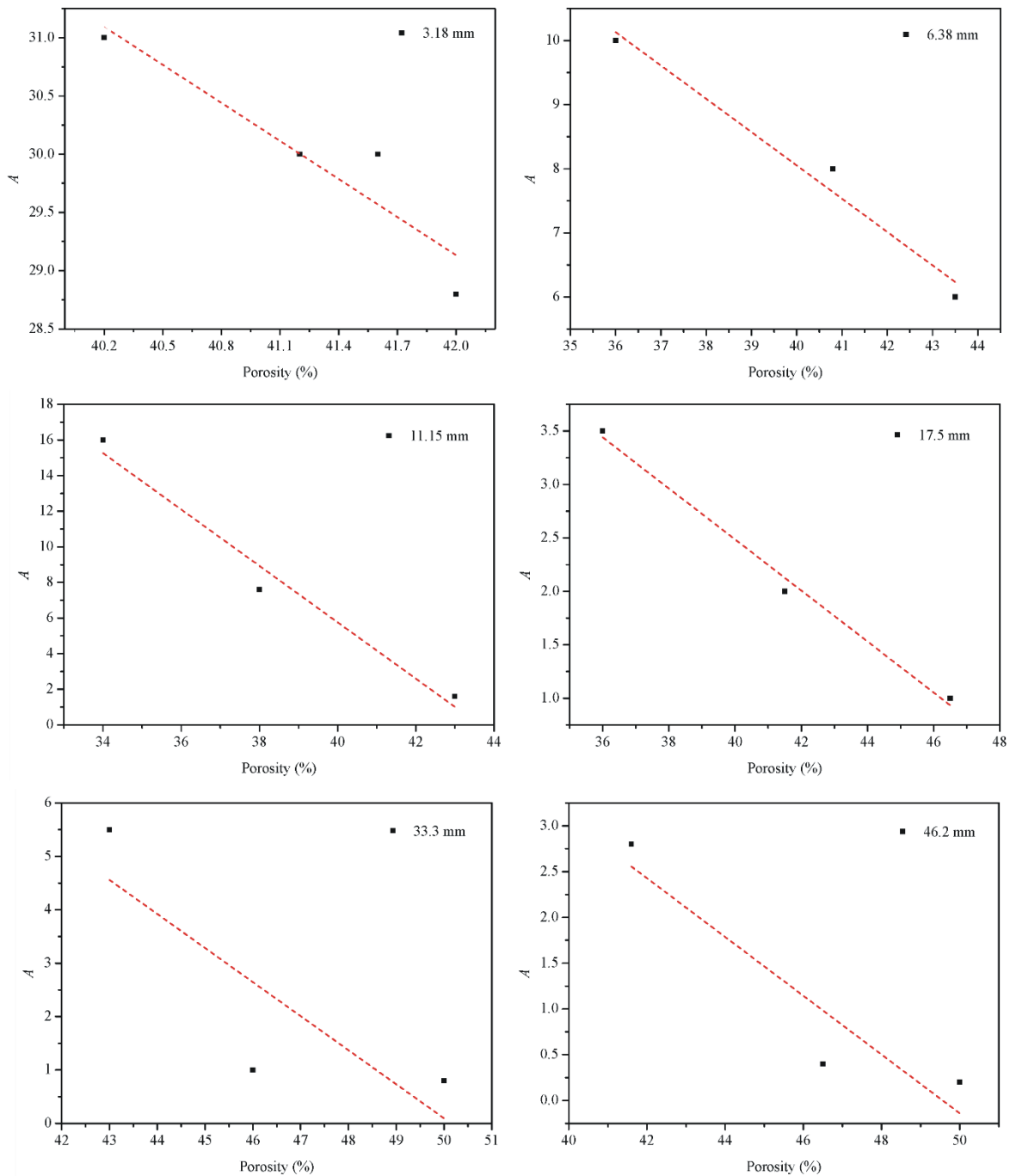
546

547

548

However, the structure of natural porous media is much more complex and heterogeneous than what has been shown in Figure 16, so it is difficult to quantitatively describe the effect of sorting degree and arrangement on seepage law.





549

550

Fig. 17. Variation of  $A$  with  $n$  of six gravels with different particle sizes.

551

In view of this, we can use a macro parameter porosity ( $n$ ) to reveal the effect of sorting

552

degree and arrangement on seepage coefficient. In order to verify the correctness of the above

553

analysis results, we selected the seepage experiment results of [Niranjan \(1973\)](#) for further

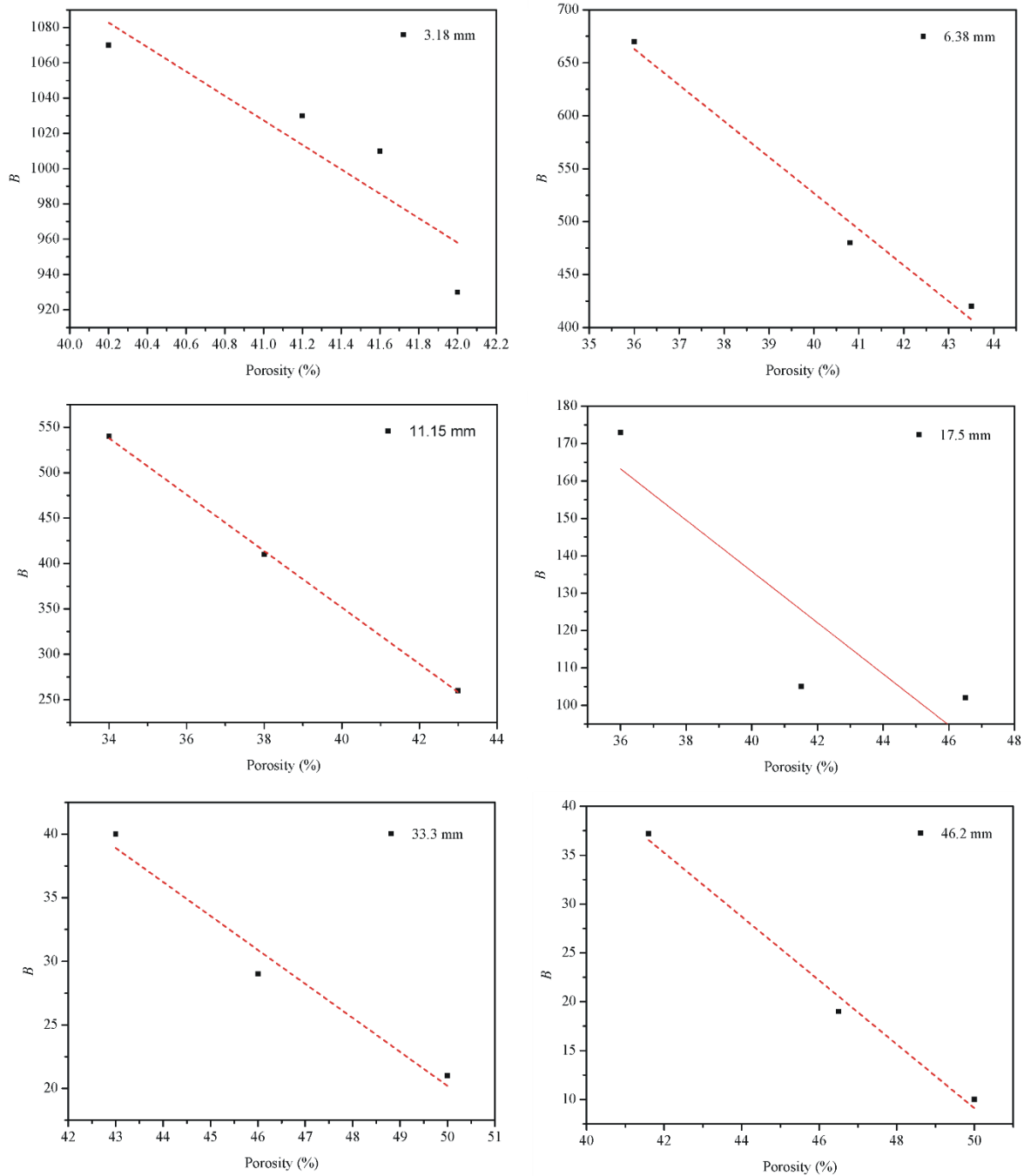
554

validation. [Niranjan \(1973\)](#) chose gravel of the same size but different porosity and carried

555

out seepage experiments. We selected the experimental results of six different particle sizes

556 with 3.18 mm, 6.38 mm, 11.15 mm, 17.5 mm, 33.3 mm and 46.2 mm from [Niranjan \(1973\)](#),  
 557 and drew the relationship between coefficient  $A$  and  $B$  and porosity respectively, as shown in  
 558 Fig. 17 and Fig. 18. We can see that the coefficients  $A$  and  $B$  of the six groups of experimental  
 559 data of [Niranjan \(1973\)](#) decrease with the increase of porosity, which is consistent with our  
 560 theoretical analysis of this investigation.



561

562

Fig. 18. Variation of  $B$  with  $n$  of six gravels with different particle sizes.

#### 563 4. Summary and conclusions

564 This study presents experimental results of Forchheimer flow in four different  
565 permeable stones with different mesh sizes, including 24 mesh size (0.71 mm), 46 mesh size  
566 (0.36 mm), 60 mesh size (0.25 mm), 80 mesh size (0.18 mm). The effects of mean pore size  
567 and pore size distribution on the transition of flow regimes (from pre-Darcian to post-Darcian)  
568 are discussed. In addition, the mercury injection experiment is proposed to investigate the  
569 pore distribution of the permeable stones. In addition, the Forchheimer coefficients are  
570 specifically discussed. The main conclusions can be summarized as follows:

571 1) The relationships between specific discharge ( $q$ ) and the "pseudo" hydraulic conductivity  
572 ( $K$ ) (which is computed as a ratio of  $q$  and hydraulic gradient,  $J$ ) of permeable stones show  
573 that deviation from Darcian flow regime is clearly visible. In addition, the critical specific  
574 discharge corresponding to the transition of flow regimes (from pre-Darcian to post-Darcian)  
575 increases with the increase of mean particle size.

576 2) When the specific discharge is small, only a small fraction of the water flowing through  
577 the pores. The rest of the water adheres to the surface of the solid particles (immobile),  
578 partially blocking the flow pathways. As the specific discharge increases, more water  
579 becomes mobile and participates in flow. Hence, the "pseudo" hydraulic conductivity  
580 increases with the increase of specific discharge. When the specific discharge increases to the  
581 critical specific discharge ( $q_c$ ), the "pseudo" hydraulic conductivity is maximized, and then it  
582 begins to decrease as the specific discharge continues to increase.

583 3) The mercury injection experiment results show that the mercury injection curve can be  
584 divided into three segments. The beginning and end segments of the mercury injection curve  
585 of the four permeable stones with different particle sizes are very gentle, while the main (or  
586 intermediate) mercury injection curve is steep, indicating that the pore size distribution falls  
587 within a narrow range, and the proportions of large pores and small pores are relatively small.

588 4) The porosity decreases as the mean particle size of permeable stone increases while the  
589 mean pore diameter increases. And the porosity can reflect the influence of particle diameter,  
590 sorting degree and arrangement mode of porous medium on seepage parameters. The larger  
591 porosity leads to the smaller coefficients  $A$  and  $B$  under the condition of the same particle size.  
592 5) The coefficient  $A$  is linearly related to  $1/d^2$  and the relationship between coefficient  $A$  and  
593  $1/d^2$  is given as  $A = 0.0025(1/d^2) + 0.003$ . The coefficient  $B$  is not linearly related to  $1/d$ ,  
594 instead it is quadratic related to  $1/d$  as  $B = 1.14E-06(1/d)^2 - 1.26E-06(1/d)$ . The particle  
595 shape and arrangement of permeable stone have imposed great influences on the seepage  
596 parameters.

597 **Notation**

598	$q$	The specific discharge, m/d.
599	$K$	The Hydraulic conductivity, m/d.
600	$J$	The dimensionless parameter defined as hydraulic gradient.
601	$A$	The Forchheimer equation coefficient (viscous force item), $\text{sm}^{-1}$ .
602	$B$	The Forchheimer equation coefficient (Inertia force item), $\text{s}^2\text{m}^{-2}$ .
603	$P_c$	The capillary force, $Pa$ .
604	$P_{50}$	The corresponding pressure value when the saturation reaches 50%, $MPa$ .
605	$P_A, P_B, P_C$	The pressure corresponding to different stages on mercury injection curve, $MPa$ .
606	$\sigma$	The solid-liquid interfacial tension.
607	$\theta$	The wet angle between the liquid and the solid surface.
608	$r$	The radius of curvature in capillary, mm.
609	$d$	The particle size, mm.

610  $d_{50}$  The mean particle sizes (50% by weight), mm.  
611  $R_m$  The mean pore diameter,  $\mu m$ .  
612  $R_{50}$  The pore diameter corresponding to the median pressure  $P_{50}$ ,  $\mu m$ .  
613  $H$  The height of the peak of the mercury injection curve.  
614  $x_c$  The abscissa corresponding to the peak of the curve (the pore size).  
615  $w$  The standard variance.  
616  $n$  The porosity.  
617  $J_n$  The viscous force-related component.  
618  $J_r$  The inertia force-related component.

#### 619 **Authors contributions**

620 Zhongxia Li: Experiment, Writing original draft. Junwei Wan: Methodology,  
621 Conceptualization. Tao Xiong: Data curation, Investigation, Experiment. Hongbin Zhan:  
622 Methodology, Writing, Review & Editing. Linqing He: Experiment, Methodology. Kun  
623 Huang: Funding acquisition, Investigation

#### 624 **Competing interests**

625 The authors declare that they have no conflict of interest.

#### 626 **Acknowledgements**

627 This study was supported by the National Natural Science Foundation of China (Grant  
628 Nos. 41402204), the National Key Research and Development Program of China  
629 (No. 2018YFC0604202) and the Fundamental Research Funds for National Universities,  
630 China University of Geosciences (Wuhan). Thank Zhongzhi Shen of China University of  
631 Geosciences for his great help in developing the experimental set up. And the authors want to

632 express their sincere appreciation of the constructive comments made by the three  
633 anonymous reviewers and Associate Editor for improving the quality of the manuscript.

## 634 **References**

- 635 Alvarez, A. E., Mahmoud, E., Martin, A. E., Masad, E., and Estakhri, C.: Stone-on-stone contact of permeable  
636 friction course mixtures, *Journal of Materials in Civil Engineering*, 22, 1129-1138,  
637 [https://doi.org/10.1061/\(ASCE\)MT.1943-5533.0000117](https://doi.org/10.1061/(ASCE)MT.1943-5533.0000117), 2010.
- 638 Anovitz, L. M. and Cole, D. R.: Characterization and Analysis of Porosity and Pore Structures, *Reviews in*  
639 *Mineralogy and Geochemistry*, 80, 61-164, <https://doi.org/10.2138/rmg.2015.80.04>, 2015.
- 640 Bear, J.: *Dynamics of Fluids in Porous Media*, American Elsevier Pub. Co., New York, N.Y., and  
641 Amsterdam, 1972.
- 642 Beavers, G. S., Sparrow, E., and Rodenz, D. E.: Influence of Bed Size on the Flow Characteristics and Porosity  
643 of Randomly Packed Beds of Spheres, *Journal of Applied Mechanics*, 40, 655-660,  
644 <https://doi.org/10.1115/1.3423067>, 1972.
- 645 Blick, E.: Capillary-Orifice Model for High-Speed Flow through Porous Media, *Industrial Engineering*  
646 *Chemistry Process Design Development*, 5, 90-94, <https://doi.org/10.1021/i260017a019>, 1966.
- 647 Bu, S., Yang, J., Dong, Q., and Wang, Q.: Experimental study of transition flow in packed beds of spheres with  
648 different particle sizes based on electrochemical microelectrodes measurement, *Applied Thermal Engineering*,  
649 73, 1525-1532, 2014.
- 650 Darcy, H.: *Recherches expérimentales relatives au mouvement de l'eau dans les tuyaux*, Impr. Impériale, Paris,  
651 France, 1857.
- 652 Dejam, M., Hassanzadeh, H., and Chen, Z.: Pre-Darcy flow in porous media, *Water Resources Research*, 53,  
653 8187-8210, <https://doi.org/10.1002/2017WR021257>, 2017.
- 654 Dudgeon, C. R.: An experimental study of the flow of water through coarse granular media, *La Houille Blanche*,  
655 785-801, <https://doi.org/10.1051/lhb/1966049>, 1966.
- 656 Dybbs, A. and Edwards, R.: A new look at porous media fluid mechanics—Darcy to turbulent, in: *Fundamentals*  
657 *of transport phenomena in porous media*, Springer, 199-256, 1984.
- 658 Ergun, S.: Fluid flow through packed columns, *Chemical Engineering Progress*, 89-94,  
659 [https://doi.org/10.1016/0009-2509\(53\)80048-5](https://doi.org/10.1016/0009-2509(53)80048-5), 1952.
- 660 Fancher, G. H. and Lewis, J. A.: Flow of simple fluids through porous materials, *Industrial & Engineering*  
661 *Chemistry*, 25, 1139-1147, <https://doi.org/10.1021/ie50286a020>, 1933.
- 662 Fetter, C. W.: *Applied Hydrogeology: International Edition*, Prentice Hall, Pearson, Engelwood Cliffs, 2001.
- 663 Forchheimer, P.: *Wasserbewegung durch boden*, Z. Ver. Deutsch, Ing., 45, 1728-1782, 1901.
- 664 Geertsma, J.: Estimating the Coefficient of Inertial Resistance in Fluid Flow Through Porous Media, *Society of*  
665 *Petroleum Engineers Journal*, 14, 445-450, <https://doi.org/10.2118/4706-PA>, 1974.
- 666 Guan, X., Wang, J., and Xiao, F.: Sponge city strategy and application of pavement materials in sponge city,  
667 *Journal of Cleaner Production*, 127022, <https://doi.org/10.1016/j.jclepro.2021.127022>, 2021.
- 668 Hall, P. L., Mildner, D., and Borst, R. L.: Small-angle scattering studies of the pore spaces of shaly rocks,  
669 *Journal of Geophysical Research Atmospheres*, 91, 2183-2192, <https://doi.org/10.1029/JB091iB02p02183>, 1986.
- 670 Han, D., Wei, L., and Zhang, J.: Experimental study on performance of asphalt mixture designed by different

671 method, *Procedia engineering*, 137, 407-414, <https://doi.org/10.1016/j.proeng.2016.01.275>, 2016.

672 Harlan, J., Picot, D., Loll, P., and Garavito, R.: Calibration of size-exclusion chromatography: use of a double  
673 Gaussian distribution function to describe pore sizes, *Analytical biochemistry*, 224, 557-563,  
674 <https://doi.org/10.1006/abio.1995.1087>, 1995.

675 Hea, X. and Zhangb, Z.: Microscopic Pore Structural Characteristics in Coal Particles, International Conference  
676 on Material, Guangzhou, China,

677 Huang, K.: Exploration of the basic seepage equation in porous media, PhD dissertation, 2012.

678 Huang, K., Wan, J., Chen, C., Linqing, H., Mei, W., and Zhang, M.: Experimental investigation on water flow in  
679 cubic arrays of spheres, *Journal of Hydrology*, 492, 61-68, <https://doi.org/10.1016/j.jhydrol.2013.03.039>, 2013.

680 Irmay, S.: Theoretical models of flow through porous media, RILEM Symp. Transfer of Water in porous media,  
681 Paris, Bull. RILEM, 29, 37-43, 1964.

682 Izbash, S.: *O Filtracii V Kropnozernstom Materiale*, Leningrad, USSR, 1931.

683 Javadi, M., Sharifzadeh, M., Shahriar, K., and Mitani, Y.: Critical Reynolds number for nonlinear flow through  
684 rough walled fractures: The role of shear processes, *Water Resources Research*, 50, 1789-1804,  
685 <https://doi.org/10.1002/2013WR014610>, 2014.

686 Jeon, H., Cho, H., Kim, J., and Sung, B.: Non-Gaussian rotational diffusion in heterogeneous media, *Physical  
687 Review E Statistical Nonlinear & Soft Matter Physics*, 90, 042105, <https://doi.org/10.1103/PhysRevE.90.042105>,  
688 2014.

689 Kadlec, R. H. and Knight, R. L.: *Treatment Wetlands*, Lewis Pub, Boca Raton, 1996.

690 Kate, J. M. and Gokhale, C. S.: A simple method to estimate complete pore size distribution of rocks,  
691 *Engineering Geology*, 84, 48-69, <https://doi.org/10.1016/j.enggeo.2005.11.009>, 2006.

692 Koch, D. and Ladd, A.: Moderate Reynolds number flows through periodic and random arrays of aligned  
693 cylinders, *Journal of Fluid Mechanics*, 349, 31-66, <https://doi.org/10.1017/S002211209700671X>, 1996.

694 Kovács, G.: *Seepage Hydraulics, Development in Water Sciences*. Elsevier: New York, 1981.

695 Latifi, M., Midoux, N., Storck, A., and Gence, J.: The use of micro-electrodes in the study of the flow regimes in  
696 a packed bed reactor with single phase liquid flow, *Chemical engineering science*, 44, 2501-2508, 1989.

697 Li, Q., Wang, F., Yu, Y., Huang, Z., Li, M., and Guan, Y. J. J. o. E. M.: Comprehensive performance evaluation  
698 of LID practices for the sponge city construction: a case study in Guangxi, China, *Journal of Environmental  
699 Management*, 231, 10-20, <https://doi.org/10.1016/j.jenvman.2018.10.024>, 2019a.

700 Li, Z., Wan, J., Huang, K., Chang, W., and He, Y.: Effects of particle diameter on flow characteristics in sand  
701 columns, *International Journal of Heat & Mass Transfer*, 104, 533-536,  
702 <https://doi.org/10.1016/j.ijheatmasstransfer.2016.08.085>, 2017.

703 Li, Z., Wan, J., Zhan, H., Cheng, X., Chang, W., and Huang, K.: Particle size distribution on Forchheimer flow  
704 and transition of flow regimes in porous media, *Journal of Hydrology*, 574, 1-11,  
705 <https://doi.org/10.1016/j.jhydrol.2019.04.026>, 2019b.

706 Lindquist, E.: On the flow of water through porous soil, Premier Congres des grands barrages (Stockholm)1933.

707 Lindquist, W. B., Venkatarangan, A., Dunsmuir, J., and Wong, T. F.: Pore and throat size distributions measured  
708 from synchrotron X-ray tomographic images of Fontainebleau sandstones, *Journal of Geophysical Research  
709 Solid Earth*, 105, 21509-21527, <https://doi.org/10.1029/2000JB900208>, 2000.

710 Maalal, O., Prat, M., Peinador, R., and Lasseux, D.: Determination of the throat size distribution of a porous  
711 medium as an inverse optimization problem combining pore network modeling and genetic and hill climbing  
712 algorithms, *Physical Review E*, 103, 023303, <https://doi.org/10.1103/PhysRevE.103.023303>, 2021.

713 Macdonald, I., El-Sayed, M., Mow, K., and Dullien, F.: Flow through porous media-the Ergun equation revisited,  
714 Industrial & Engineering Chemistry Fundamentals, 18, 199-208, <https://doi.org/10.1021/i160071a001>, 1979.

715 Moutsopoulos, K. N., Papaspyros, I. N., and Tsihrintzis, V. A.: Experimental investigation of inertial flow  
716 processes in porous media, Journal of hydrology, 374, 242-254, <https://doi.org/10.1016/j.jhydrol.2009.06.015>,  
717 2009.

718 Niranjan, H.: Non-Darcy flow through porous media, M.S., dissertation, ITT, Kanpur, India, 1973.

719 Panfilov, M. and Fourar, M.: Physical splitting of nonlinear effects in high-velocity stable flow through porous  
720 media, Advances in Water Resources, 29, 30-41, <https://doi.org/10.1016/j.advwatres.2005.05.002>, 2006.

721 Pittman, E. D.: Relationship of porosity and permeability to various parameters derived from mercury injection-  
722 capillary pressure curves for sandstone (1), AAPG bulletin, 76, 191-198, [https://doi.org/10.1306/BDF87A4-  
723 1718-11D7-8645000102C1865D](https://doi.org/10.1306/BDF87A4-1718-11D7-8645000102C1865D), 1992.

724 Prowell, B. D., Allen Cooley Jr, L., and Schreck, R. J.: Virginia's experience with 9.5-mm nominal-maximum-  
725 aggregate-size stone matrix asphalt, Transportation research record, 1813, 133-141,  
726 <https://doi.org/10.3141/1813-16>, 2002.

727 Rezaee, R., Saeedi, A., and Clennell, B.: Tight gas sands permeability estimation from mercury injection  
728 capillary pressure and nuclear magnetic resonance data, Journal of Petroleum Science and Engineering, 88, 92-  
729 99, <https://doi.org/10.1016/j.petrol.2011.12.014>, 2012.

730 Rijfkoogel, L. S., Ghanbarian, B., Hu, Q., and Liu, H. H.: Clarifying pore diameter, pore width, and their  
731 relationship through pressure measurements: A critical study, Marine and Petroleum Geology, 107, 142-148,  
732 <https://doi.org/10.1016/j.marpetgeo.2019.05.019>, 2019.

733 Scheidegger, A.: The physics of flow through porous media,  
734 Scheidegger, A. E.: On the stability of displacement fronts in porous media: a discussion of the muskat-  
735 aronofsky model, Canadian Journal of Physics, 38, 153-162, <https://doi.org/10.1139/p60-017>, 1960.

736 Scheidegger, A. E.: The physics of flow through porous media, University of Toronto Press,  
737 <https://doi.org/10.3138/9781487583750>, 2020.

738 Schmitt, M., Fernandes, C. P., da Cunha Neto, J. A., Wolf, F. G., and dos Santos, V. S.: Characterization of pore  
739 systems in seal rocks using nitrogen gas adsorption combined with mercury injection capillary pressure  
740 techniques, Marine and Petroleum Geology, 39, 138-149, <https://doi.org/10.1016/j.marpetgeo.2012.09.001>, 2013.

741 Schneebeil, G.: Experiences sur la limite de validite de la loi de Darcy et l'apparition de la turbulence dans un  
742 ecoulement de filtration, La Huille Blanche, 2, 141-149, <https://doi.org/10.1051/lhb/1955030>, 1955.

743 Sedghi-Asl, M., Rahimi, H., and Salehi, R.: Non-Darcy Flow of Water Through a Packed Column Test,  
744 Transport in Porous Media, 101, 215-227, <https://doi.org/10.1007/s11242-013-0240-0>, 2014.

745 Seguin, D., Montillet, A., Comiti, J., and Huet, F.: Experimental characterization of flow regimes in various  
746 porous media—II: Transition to turbulent regime, Chemical engineering science, 53, 3897-3909, 1998.

747 Shi, W., Yang, T., and Yu, S.: Experimental Investigation on Non-Darcy Flow Behavior of Granular Limestone  
748 with Different Porosity, Journal of Hydrologic Engineering, 25, 06020004,  
749 [https://doi.org/10.1061/\(ASCE\)HE.1943-5584.0001966](https://doi.org/10.1061/(ASCE)HE.1943-5584.0001966), 2020.

750 Sidiropoulou, M. G., Moutsopoulos, K. N., and Tsihrintzis, V.: Determination of Forchheimer equation  
751 coefficients a and b, Hydrological Processes, 21, 534-554, <https://doi.org/10.1002/hyp.6264>, 2007.

752 Skjetne, E., Hansen, A., and Gudmundsson, J.: High-velocity flow in a rough fracture, Journal of Fluid  
753 Mechanics, 383, 1-28, <https://doi.org/10.1017/S0022112098002444>, 1999.

754 Soni, J., Islam, N., and Basak, P.: An experimental evaluation of non-Darcian flow in porous media, Journal of



755 Hydrology, 38, 231-241, [https://doi.org/10.1016/0022-1694\(78\)90070-7](https://doi.org/10.1016/0022-1694(78)90070-7), 1978.

756 Souto, H. P. A. and Moyne, C.: Dispersion in two-dimensional periodic porous media. Part I. Hydrodynamics,  
757 Physics of Fluids, 9, 2243-2252, <https://doi.org/10.1063/1.869365>, 1997.

758 Suo, Z., Bao, X., Nie, L., Yan, Q., and Qi, K.: Optimization Design of Mix Proportion of Large Stone Permeable  
759 Mixture Based on Target Air Voids, Buildings, 11, 514, <https://doi.org/10.3390/buildings11110514>, 2021.

760 Swartzendruber, D.: Modification of Darcy's law for the flow of water in soils, Soil Science, 93, 22-29,  
761 <https://doi.org/10.1097/00010694-196201000-00005>, 1962a.

762 Swartzendruber, D.: Non-Darcy flow behavior in liquid-saturated porous media, Journal of Geophysical  
763 Research, 67, 5205-5213, <https://doi.org/10.1029/JZ067i013p05205>, 1962b.

764 Van Lopik, J. H., Zazai, L., Hartog, N., and Schotting, R.: Nonlinear Flow Behavior in Packed Beds of Natural  
765 and Variably Graded Granular Materials, Transport in Porous Media, 131, 957-983,  
766 <https://doi.org/10.1007/s11242-019-01373-0>, 2019.

767 Van Lopik, J. H., Snoeijers, R., van Dooren, T. C. G. W., Raoof, A., and Schotting, R. J.: The Effect of Grain  
768 Size Distribution on Nonlinear Flow Behavior in Sandy Porous Media, Transport in Porous Media, 120, 1-30,  
769 <https://doi.org/10.1007/s11242-017-0903-3>, 2017.

770 Wang, J., Ng, P.-L., Gong, Y., Su, H., and Du, J.: Experimental Study of Low Temperature Performance of  
771 Porous Asphalt Mixture, Applied Sciences, 11, 4029, <https://doi.org/10.3390/app11094029>, 2021.

772 Ward, J. C.: Turbulent Flow in Porous Media, Journal of Hydraulic Engineering, 90, 1-12,  
773 [http://dx.doi.org/10.1016/S0301-9322\(02\)00051-4](http://dx.doi.org/10.1016/S0301-9322(02)00051-4), 1964.

774 Washburn, E. W.: The Dynamics of Capillary Flow, Physical Review, 17, 273-283,  
775 <https://doi.org/10.1103/PhysRev.17.273>, 1921.

776 Wright, D.: Nonlinear Flow Through Granular Media, Journal of Hydraulic Engineering, 94, 851-872,  
777 <https://doi.org/10.1061/JYCEAJ.0001858>, 1968.

778 Xie, H. and Watson, D. E.: Determining air voids content of compacted stone matrix asphalt mixtures,  
779 Transportation research record, 1891, 203-211, <https://doi.org/10.3141/1891-24>, 2004.

780 Xu, C. and Torres-Verdín, C.: Pore System Characterization and Petrophysical Rock Classification Using a  
781 Bimodal Gaussian Density Function, Mathematical Geosciences, 45, 753-771, [https://doi.org/10.1007/s11004-](https://doi.org/10.1007/s11004-013-9473-2)  
782 [013-9473-2](https://doi.org/10.1007/s11004-013-9473-2), 2013.

783 Yang, B., Yang, T., Xu, Z., Liu, H., Yang, X., and Shi, W.: Impact of Particle-Size Distribution on Flow  
784 Properties of a Packed Column, Journal of Hydrologic Engineering, 24, 04018070,  
785 [https://doi.org/10.1061/\(ASCE\)HE.1943-5584.0001735](https://doi.org/10.1061/(ASCE)HE.1943-5584.0001735), 2019.

786 Yu, T., Liu, D., Zhang, H., and Wang, H.: Influence of pore water phase change on service performance for  
787 permeable pavement in Sponge City, Water Science and Technology, 84, 3769-3779,  
788 <https://doi.org/10.2166/wst.2021.459>, 2021.

789 Zeng, Z. and Grigg, R.: A criterion for non-Darcy flow in porous media, Transport in porous media, 63, 57-69,  
790 <https://doi.org/10.1007/s11242-005-2720-3>, 2006.

791 Zhen-hua, MIN, and, Min, CAO, and, Shu, ZHANG, and, and Xiu-dan: Effect of precursor on the pore structure  
792 of carbon foams, New Carbon Materials, 22, 75-79, [https://doi.org/10.1016/S1872-5805\(07\)60009-2](https://doi.org/10.1016/S1872-5805(07)60009-2), 2007.

793 Zhihong, L. I., Jihong, S., Dong, W. U., Yuhan, S., Liu, Y. I., Wenjun, S., and Baozhong, D.: Determination of  
794 average pore diameter of SiO<sub>2</sub> xerogels by small angle X-ray scattering, ACTA Physica sinica, 49, 1312-1315,  
795 <https://doi.org/10.3321/j.issn:1000-3290.2000.07.020>, 2000.

796 Zhou, H., Fang, Y.-g., Chen, M., Gu, R.-g., and Li, W.: Experimental and analytical study on electro-osmosis in

797 low-permeability soil considering the pore size effect, *Geotechnique*, 71, 141-152,  
798 <https://doi.org/10.1680/jgeot.18.p.362>, 2019.

799

800

801